*Mathematical Biosciences and Engineering*

http://www.aimspress.com/journal/MBE

MBE, 22(10): 2720–2760.
DOI: 10.3934/mbe.2025100
Received: 05 May 2025
Revised: 30 June 2025
Accepted: 15 July 2025
Published: 27 August 2025

*Research article*

# Backward bifurcation and periodic dynamics in a tuberculosis model with integrated control strategies

**Dipo Aldila[1,2,*], Chidozie Williams Chukwu[3], Eka D. A. Ginting[1], F. Fatmawati[4], Faishal Farrel Herdicho[4], Mohammad Ivan Azis[5] and S. Sutrisno[6]**

[1] Department of Mathematics, Faculty of Mathematics and Natural Sciences, Universitas Indonesia, Depok 16424, Indonesia

[2] Innovative Mathematics and Predictive Analytics for Complex System and Technology Laboratory (IMPACT Lab), Universitas Indonesia, Depok 16424, Indonesia

[3] Department of Mathematical Sciences, Georgia Southern University, 65 Georgia Ave., P.O. Box 8093, Statesboro, Georgia 30460, USA

[4] Department of Mathematics, Faculty of Science and Technology, Universitas Airlangga, Surabaya, Indonesia

[5] Department of Mathematics, Hasanuddin University, Makassar, Indonesia

[6] Department of Mathematics, Diponegoro University, Tembalang, Semarang 50275, Indonesia

* **Correspondence:** Email: aldiladipo@sci.ui.ac.id.

**Abstract:** In this study, we present a unified mathematical model for tuberculosis (TB) that integrates key interventions: Mask use and media campaigns to raise community awareness and promote vaccine booster uptake. The model also incorporates slow–fast disease progression and limited treatment capacity. A mathematical analysis was conducted to determine the existence and stability of equilibrium points. From the mathematical analysis on the stability criteria of the TB-free equilibrium point, we show that TB can be eradicated if the basic reproduction number is below one. However, due to insufficient treatment capacity, a backward bifurcation may occur when the reproduction number equals one, enabling the coexistence of endemic and disease-free equilibria even when the reproduction number is below one. The parameter estimation is based on TB incidence data per 100,000 individuals in Indonesia. Sensitivity analysis revealed that although both interventions are effective, media campaigns combined with vaccine boosters are more impactful in reducing TB transmission than the use of masks. Numerical simulations further suggest the possibility of periodic outbreaks, indicating potential seasonal TB patterns. To explore adaptive intervention strategies, we extended the model using an optimal control framework. Our findings suggested that combined implementation of face masks and media campaigns is more effective than using either alone, particularly when the likelihood of rapid disease progression increases.

**Keywords:** tuberculosis; media campaign; face mask; parameter estimation; global sensitivity analysis; periodic solution; optimal control model

## 1. Introduction

Tuberculosis (TB) is a contagious bacterial infection caused by *Mycobacterium tuberculosis* [1–3]. It primarily affects the lungs (pulmonary TB) but can also impact other parts of the body (extrapulmonary TB) [1, 2]. The symptoms of pulmonary TB include a persistent cough, chest pain, and coughing up blood. Other general symptoms are fever, night sweats, weight loss, and fatigue [2]. TB remains a major global health challenge. According to the World Health Organization (WHO), TB is one of the top 10 causes of death worldwide and the leading cause of a single infectious agent, surpassing HIV/AIDS [4, 5]. In the year 2020, an estimated 10 million people fell ill with TB, and 1.4 million died from the disease [6]. In 2022, TB was responsible for approximately 1.3 million deaths, including 167,000 among people with HIV [4, 5]. This makes it the second leading infectious disease killer after COVID-19. Additionally, an estimated 10.6 million people fell ill with TB globally in 2022 [4, 5]. The burden is disproportionately high in low- and middle-income countries, with significant impacts on vulnerable populations such as people living with HIV, children, and the elderly [7]. TB infection can be categorized into two major forms: Latent TB infection (LTBI) and active TB disease. Individuals with LTBI carry the bacteria but do not exhibit symptoms and are not infectious [1]. However, they are at risk of developing active TB, particularly if their immune system becomes compromised. Active TB occurs when the bacteria overcomes the immune defenses, leading to symptomatic and infectious disease [8]. The concept of slow-fast progression in TB highlights the differing rates at which LTBI can progress to active TB [1, 9, 10]. Slow progression refers to the gradual activation of the disease over months or years, often in individuals with weakened immune systems [1, 9]. In contrast, fast progression occurs rapidly, usually within weeks to months after initial infection, and is more common in young children and those with HIV [9].

Interventions for TB control are accomplished by focusing on preventing transmission, ensuring effective treatment, and enhancing public awareness. Community awareness campaigns are essential in educating the public about TB symptoms, transmission routes, and the importance of early diagnosis and treatment adherence. These campaigns can significantly reduce the stigma associated with the disease, encouraging individuals to seek medical attention promptly. Effective campaigns utilize media channels, including radio, television, and social media, to reach diverse populations [11]. Treatment for TB typically involves a rigorous six-month course of a combination of antimicrobial drugs, including isoniazid, rifampin, pyrazinamide, and ethambutol [12, 13]. Adherence to this treatment regimen is crucial to ensure complete eradication of the bacteria and to prevent the development of drug-resistant TB strains. The WHO endorses the Directly Observed Treatment, Short-course (DOTS) strategy to improve treatment adherence. Under DOTS, healthcare workers or trained volunteers observe and support patients in taking their medication, thereby reducing the likelihood of incomplete treatment and enhancing treatment success rates [14]. In areas with high TB prevalence, saturated treatment approaches are employed. These strategies involve intensive case-finding and treatment efforts, ensuring that even those with LTBI receive appropriate

therapy to prevent progression to active TB. Saturated treatment approaches also include the provision of prophylactic treatment to individuals at high risk, such as those with HIV, which significantly reduces the incidence of TB in these vulnerable populations [15]. Comprehensive public health interventions form an integrated approach to TB control and eradication. This includes vaccination with the Bacillus Calmette-Guérin vaccine, contact tracing, and community-based treatment initiatives.

Mathematical modeling has become an essential tool for understanding tuberculosis (TB) transmission and evaluating control strategies. Athithan and Ghosh [16] developed a model to assess the effects of case detection and treatment, incorporating progression from latent to active TB, diagnostic effectiveness, and treatment success rates. Their simulations showed that improving case detection and treatment adherence can significantly reduce TB incidence and prevalence, underscoring the importance of early diagnosis and effective therapy. Building on this, Aldila et al. [17] proposed a model to understand the impact of the novel M72/AS01E vaccine for TB prevention. Their model reveals rich dynamics which trigger from several infection pathways, such as relapse and reinfection. Just recently, Aldila et al. [1] examined the impact of medical mask usage and improved case detection across multiple countries through a cost-effectiveness analysis. Their findings revealed that these combined interventions not only significantly lower TB transmission rates but also offer a cost-efficient strategy applicable in various healthcare settings. Together, these studies highlight the power of mathematical models in informing evidence-based TB control policies.

Several researchers have incorporated biological heterogeneity into TB transmission models, particularly by distinguishing fast and slow progression pathways to active disease. For instance, Song et al. [9] developed a compartmental model that stratifies the population into susceptible, exposed, infectious, and recovered individuals, and further subdivides the infectious class into fast and slow progressors. Their model also accounts for contact heterogeneity by differentiating close and casual interactions. Through stability analysis and numerical simulations, they demonstrated the significant role of casual contacts in TB transmission, particularly in densely populated urban environments. Building on the idea of progression heterogeneity, Zhang et al. [18] extended the modeling framework by incorporating the impact of media coverage on public awareness and behavioral response. Their model includes similar compartments for susceptible, exposed, fast-progressing, slow-progressing, and recovered individuals, but introduces additional parameters to capture the influence of media on disease transmission and control. Their results highlight that enhanced public awareness through media campaigns can lead to earlier diagnosis and treatment, thereby reducing the overall transmission rate. These two studies are discussed together because they address a common structural feature, progression pathways, while each integrates a different real-world complexity: Contact structure in the case of Song et al. [9] and behavioral awareness in the case of Zhang et al. [18]. Taken together, they illustrate how biological and social heterogeneities can be embedded into TB models to better reflect the dynamics observed in real populations. This synthesis provides a foundation for further model development that seeks to integrate additional intervention strategies and inform more comprehensive TB control policies.

Several mathematical models have been developed to study the transmission dynamics of tuberculosis (TB), incorporating aspects such as slow and fast disease progression and the effects of various intervention strategies. These strategies include media and education campaigns, the use of masks, treatment programs, and general control measures. For instance, Athithan and Ghosh [16]

focused on case detection and treatment, while Avilov et al. [19] explored progression using fluorography data. Sumner and White [20] evaluated the impact of preventive therapy, and Chong et al. [21] examined the treatment of latent TB infection in the elderly. Other studies considered differential infectivity [22], age-dependent latency and fast-slow progression [10], treatment interruptions with dual latent periods [23], and differences in awareness levels affecting susceptibility and progression [24]. Additionally, models have incorporated fractional-order stochastic dynamics [3], parameter estimation for TB spread in East Java, Indonesia [25], and multidrug-resistant TB [26], among others. These diverse modeling approaches underscore the complexity of TB as a disease influenced by numerous internal and external factors, ranging from individual immune response to population-level awareness and treatment access. Despite extensive research and control efforts, TB remains a major global health concern, as the number of cases has not declined significantly, highlighting the ongoing need for comprehensive and innovative approaches to its control.

Based on the literature reviewed, it is evident that TB is a highly complex disease. Incorporating all critical factors, such as slow-fast progression of infection, various intervention strategies, vaccination, multi-drug resistance, coinfection with other diseases, and many other factors, leads to more complex models. A good mathematical model should ideally represent real-world situations as closely as possible, but this often results in increased model complexity. Therefore, there must be a balance between model complexity and the specific research question being addressed.

We aim to explore the impact of slow-fast progression on the effectiveness of media campaigns and face mask use as a combined TB control strategy. To the best of our knowledge, no TB mathematical models incorporate these two strategies while considering the effects of slow-fast progression and limited treatment capacity in hospitals. In this article, we introduce a compartmental model that divides the human population into five compartments: Susceptible unaware, susceptible aware, passive TB, active TB, and recovered individuals. Important factors such as media campaign, face mask use, slow-fast progression, treatment failure, and modified saturated treatment rate are included in the model. Several important findings emerged from our analysis. Notably, we found that a reproduction number smaller than one does not necessarily guarantee TB elimination. Additionally, under specific conditions related to treatment saturation, the model can produce periodic solutions that from the perspective of public health, will provide a seasonal outbreak situation. Our optimal control simulations, using parameters fitted to Indonesian data, indicate that face mask use and media campaigns should be implemented together than as single interventions. Furthermore, when more individuals experience fast TB progression, more intensive government interventions are required to ensure better outcomes in TB control programs.

The paper is organized as follows: We give the literature reviews on the TB model and the state of the art of our article in the first section. We introduce our model in Section 2, and model analysis regarding the construction of next generation matrix to find the reproduction number, and equilibrium point existence and stability analysis, are also conducted in Section 2. In Section 5, we conduct numerical experiments regarding parameter estimation and sensitivity analysis. We extend our proposed model in Section 2 as an optimal control problem in Section 6. Finally, some conclusions are given in Section 7.

## 2. Model construction and analysis

In this section, we present the construction and analysis of a mathematical model that we propose in this article. The model is formulated as a system of ordinary differential equations based on a set of assumptions and a transmission diagram that illustrates transitions between compartments. Mathematical analysis, including the existence and stability of equilibrium points, is discussed. Furthermore, the role of the reproduction number in influencing the long-term behavior of the model is examined.

### *2.1. Model construction*

Here, an epidemic model is constructed to study the dynamics of TB transmission in a population. The model considers several important factors, such as the latent stage, slow-fast progression, the use and efficacy of face masks, media campaigns to raise public awareness of TB, and the limitations of hospital treatment capacity. The total human population, denoted by $N$, is divided into five compartments: The susceptible unaware compartment ($S$), the susceptible aware compartment ($A$), the latent compartment ($L$), the infected and infectious compartment ($I$), and the recovered compartment ($R$). It is important to mention that the awareness effect $A$ here refers to the willingness of individuals to conduct any behavior that may reduce their probability to get infected by TB, such as taking a vaccine booster, conducting clean life habit, avoiding close contact with possible infected individuals, and so on. This effect will later be represented by a reduction in their infection rate, which is smaller than the unaware individuals. The model construction follows the transmission diagram given in Figure 1. Detailed descriptions of model parameters are provided in Table 1.

**Table 1.** Parameter description of the model.

| Parameter | Description | Unit |
|---|---|---|
| $\Lambda$ | Natural recruitment rate | $\frac{\text{human}}{\text{year}}$ |
| $\mu$ | Natural death rate | $\frac{1}{\text{year}}$ |
| $\beta_1$ | Infection rate of unaware susceptible individual | $\frac{1}{\text{year}\times\text{human}}$ |
| $\beta_2$ | Infection rate of aware susceptible individual | $\frac{1}{\text{year}\times\text{human}}$ |
| $u_1$ | Proportion of infected individual $I$ use face mask | - |
| $\bar{u_2}$ | Rate of media campaign | $\frac{1}{\text{year}}$ |
| $\eta$ | Drop out due to loss of awareness on TB | $\frac{1}{\text{year}}$ |
| $\xi$ | Mask efficacy | - |
| $p$ | Proportion of new infected individuals experience slow progression | - |
| $\alpha$ | Recovery rate of $L$ individuals due to early treatment | $\frac{1}{\text{year}}$ |
| $k$ | Proportion of individuals in $L$ perfectly recovered | - |
| $\gamma_m$ | Natural recovery rate of individuals in $I$ compartment | $\frac{1}{\text{year}}$ |
| $\gamma_0$ | Maximum reduction of $\gamma_m$ due to increase infected individuals who need treatment | $\frac{1}{\text{year}}$ |
| $b$ | Saturation parameter of recovery rate of individuals in $I$ compartment | $\frac{1}{\text{human}}$ |

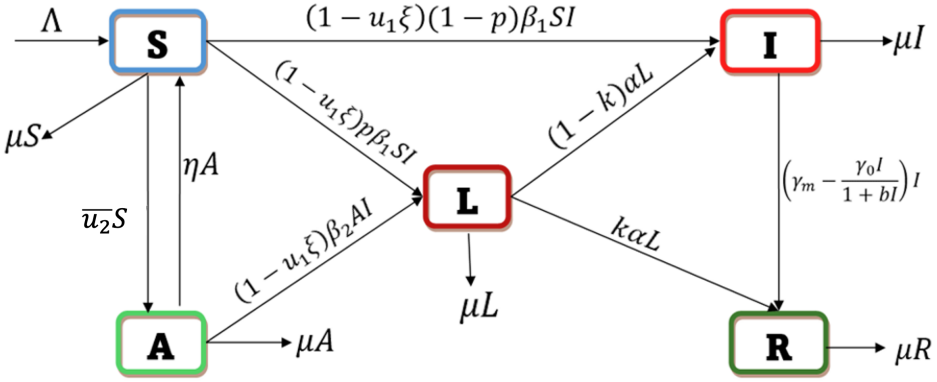


**Figure 1.** Transmission diagram of model in system (2.1).

TB is primarily transmitted through the air when infected individuals talk, cough, or sneeze, releasing droplets containing the bacterium *Mycobacterium tuberculosis*. Moreover, transmission of TB through newborns is very rare. Therefore, we assume that all newborns are born as non-infected individuals. Consequently, we describe a newborn entering the population denoted by $\Lambda$ as entering the susceptible unaware population. Another important assumption in our model is that all newborns are assumed to have received the neonatal TB vaccination. This assumption is based on policies in several countries. For example, Indonesia has mandated the Bacillus Calmette–Guérin (BCG) vaccine for newborns since 1956, incorporating it into the national immunization program. Due to a media campaign aimed at raising community awareness about the dangers of TB, we assume that individuals in the susceptible unaware compartment can become aware. This campaign includes educational programs, broader health initiatives, adaptations of preventive strategies, and increased communication strategies to address evolving societal needs. Assuming the rate of the media campaign is given by $u_2$, there is a transition rate from the susceptible unaware to the susceptible aware compartment. In reality, awareness of important issues such as TB cannot last for a lifetime. Societal changes, complacency, resource allocation issues, and other factors may cause individuals who were once aware to become unaware again. Therefore, we have a drop-out rate from aware to unaware susceptible compartment, denoted by $\eta$.

Individuals in compartments $S$ and $A$ can become infected with TB if they come into contact with TB bacteria produced by individuals in compartments $I$. We assume that individuals in the $L$ compartment not yet able spread TB due to the passive TB stage. Furthermore, it should be noted that individuals in compartment $A$ are aware and take measures to prevent TB infection, including receiving vaccinations that can reduce the chance of TB infection. Therefore, the infection rates in compartments $S$ and $A$ are different, denoted as $\beta_1$ and $\beta_2$, respectively for $S$ and $A$. Due to the effect of vaccination in compartment $A$, it is assumed that $\beta_2 < \beta_1$. In addition to interventions through media campaigns to increase community awareness, our proposed model also considers the proportion of infected individuals $I$ using masks at a proportion of $u_1$ with efficacy level $\xi$. Note that $\xi \in [0, 1]$, where $\xi = 1$ represent that the face mask can gives a 100% efficacy to block TB infection from an $I$ individual to $S$ individuals. To model the infection form, we use a bilinear incidence rate. Hence, the new infected individual in $S$ compartment is given by $(1 - u_1\xi)\beta_1 S I$, while newly infected

in compartment $A$ is given by $(1 - u_1\xi)\beta_2 AI$. This bilinear incidence form is widely adopted in tuberculosis modeling due to its analytical tractability and provides a reasonable approximation of transmission dynamics in populations with relatively stable contact patterns, such as those considered in this study. In populations with more significant heterogeneity, readers may consider using density-dependent or saturated incidence forms as alternative modeling choices.

Another important feature of our proposed model is the inclusion of slow-fast progression of TB [1, 9, 10]. Slow-fast progression refers to the varying rates at which infected individuals move through different stages of the disease. Several diseases exhibit slow-fast progression, including TB, HIV/AIDS, Hepatitis B and C, Human Papillomavirus (HPV), Chickenpox, Syphilis, and Leprosy. In the context of TB, slow progression occurs when a newly infected individual enters a latent stage before progressing to infectious/active TB. Individuals in the latent stage do not show symptoms and are not infectious. This stage can last for months, years, or a lifetime without progressing to active TB. Conversely, fast progression refers to the scenario where a newly infected individual quickly develops active TB without entering the latent stage. The incubation period for these individuals is shorter compared to those in the latent stage. Several factors can contribute to fast progression, such as a weakened immune system due to other diseases like HIV, malnutrition, or other underlying health conditions. The slow-fast progression in our model is represented by parameter $p$. Therefore, we have newly infected individuals from the $S$ compartment who experience slow progression represented as $(1 - u_1\xi)p\beta_1 SI$ to the $L$ compartment, while the fast progression directly goes to the $I$ compartment as $(1 - u_1\xi)(1 - p)\beta_1 SI$. Due to the use of vaccine boosters in the $A$ compartment, we assume that newly infected individuals from the $A$ compartment experience a slow progression when they are infected with TB.

We assume that infected individuals in the $L$ compartment may receive early treatment due to early detection. Since the symptoms are mild, it is assumed that infected individuals in the $L$ compartment do not need hospitalization. We assume they receive only home treatment to cure them from TB infection. The recovery rate due to treatment in the $L$ compartment is given by $\alpha$, where the probability of success is given by $k \in [0, 1]$. Infected individuals in the $L$ compartment who fail to recover after the treatment will move to the $I$ compartment with a probability of $1 - k$. Infected individuals in the $I$ compartment are assumed to have more severe symptoms and therefore require more intensive treatment to cure them from TB. We assume that infected individuals in the $I$ compartment can recover at a maximum rate of $\gamma_m$. However, due to the increased number of infected individuals needing treatment in the hospital, this $\gamma_m$ recovery rate can be reduced by the amount of $\frac{\gamma_0 I}{1+bI}$. This latter factor is a monotonic increasing function with respect to $I$. Therefore, as the number of infected individuals increases, $\gamma_m - \frac{\gamma_0 I}{1+bI}$ will decrease. When the number of infected individuals tends to infinity, the minimum recovery rate of $I$ individuals is given by $\gamma_m - \frac{\gamma_0}{b}$. Hence, we assume that $\gamma_m \geq \frac{\gamma_0}{b}$ to ensure that $\gamma_m - \frac{\gamma_0 I}{1+bI}$ is always non-negative for any value of $I$. Last, we assume that every compartment can decrease due to a constant natural death rate, denoted by $\mu$.

Based on the explanation of the model construction above, the TB transmission model considering factors such as slow-fast progression, media campaigns, use of vaccines booster, use of face masks, saturated treatment, and treatment failure is given by the following five-dimensional system of differential equations:

$$\begin{aligned}
\frac{dS}{dt} &= \Lambda + \eta A - (1-u_1\xi)p\beta_1 S I - (1-u_1\xi)(1-p)\beta_1 S I - \bar{u_2} S - \mu S,\\
\frac{dA}{dt} &= \bar{u_2} S - (1-u_1\xi)\beta_2 A I - \eta A - \mu A,\\
\frac{dL}{dt} &= (1-u_1\xi)p\beta_1 S I + (1-u_1\xi)\beta_2 A I - (1-k)\alpha L - k\alpha L - \mu L,\\
\frac{dI}{dt} &= (1-u_1\xi)(1-p)\beta_1 S I + (1-k)\alpha L - \left(\gamma_m - \frac{\gamma_0 I}{1+bI}\right) I - \mu I,\\
\frac{dR}{dt} &= k\alpha L + \left(\gamma_m - \frac{\gamma_0 I}{1+bI}\right) I - \mu R,
\end{aligned} \tag{2.1}$$

with initial conditions $S(0) = S_0, A(0) = A_0, L(0) = L_0, I(0) = I_0$, and $R(0) = R_0$. Since in the boundary in $\mathbb{R}^5_{\geq 0}$ we have

$$\begin{aligned}
\frac{dS}{dt} &= \Lambda + \eta A > 0,\\
\frac{dA}{dt} &= \bar{u_2} S \geq 0,\\
\frac{dL}{dt} &= (1-u_1\xi)p\beta_1 S I + (1-u_1\xi)\beta_2 A I \geq 0,\\
\frac{dI}{dt} &= (1-k)\alpha L \geq 0,\\
\frac{dR}{dt} &= k\alpha L + \left(\gamma_m - \frac{\gamma_0 I}{1+bI}\right) I \geq 0.
\end{aligned}$$

Therefore, all the rates are non-negative on the boundary planes with non-negative initial condition $S(0) = S_0, A(0) = A_0, L(0) = L_0, I(0) = I_0$, and $R(0) = R_0$. Therefore, for any non-negative initial conditions, all vector field direction is inward from the boundary planes. Hence, the solution of system (2.1) is always non-negative for all time $t > 0$. Furthermore, adding all the equations of model in (2.1) yields

$$\frac{dN}{dt} = \Lambda - \mu N. \tag{2.2}$$

With initial condition $N(0) = N_0$, the solution of (2.2) is

$$N(t) = \frac{\Lambda}{\mu}(1 - e^{-\mu t}) + N_0 e^{-\mu t}.$$

It can be seen that the solution of $N(t)$ is always on the region of

$$\Omega = \left\{(S, A, L, I, R) \in \mathbb{R}^5_{\geq 0} | 0 < N(t) \leq \max\left\{N(0), \frac{\Lambda}{\mu}\right\}\right\}.$$

Therefore, all feasible solutions of system (2.1) enter $\Omega$. This implies that $\Omega$ is an attracting set.

### *2.2. Model analysis*

In this section, we conduct a mathematical analysis of the model in system (2.1), focusing on its non-dimensionalization process, the calculation and stability analysis of equilibrium points, and the determination of the reproduction number.

2.2.1. Model non-dimensionalization

Let us assume the total of the human population is constant, by assuming that $\Lambda = \mu N$. Scaling each variable with respect to the total population $N$, we have:

$$x_1 = \frac{S}{N}, x_2 = \frac{A}{N}, x_3 = \frac{L}{N}, x_4 = \frac{I}{N}, x_5 = \frac{R}{N}.$$

Hence, we have $x_1 + x_2 + x_3 + x_4 + x_5 = 1$. Furthermore, we rescale the time scale to match the recovery rate of the $L$ compartment, denoted by $\alpha$. We assume that $\tau = t\alpha$, where $\tau$ represents the new time scale. Consequently, we introduce the following new parameters as a direct result of this time rescaling:

$$m = \frac{\mu}{\alpha}, e = \frac{\eta}{\alpha}, b_1 = \frac{\beta_1 N}{\alpha}, b_2 = \frac{\beta_2 N}{\alpha}, u_2 = \frac{\bar{u_2}}{\alpha}, d_1 = \frac{\gamma_m}{\alpha}, d_2 = \frac{\gamma_0}{\alpha}, c = \frac{1}{N}.$$

Using the above assumptions, the model in Eq (2.1) can now be written as:

$$\begin{aligned}
\frac{dx_1}{d\tau} &= m(1 - x_1) + ex_2 - (1 - u_1\xi)b_1x_1x_4 - u_2^*x_1,\\
\frac{dx_2}{d\tau} &= u_2x_1 - (1 - u_1\xi)b_2x_2x_4 - (e + m)x_2,\\
\frac{dx_3}{d\tau} &= (1 - u_1\xi)pb_1x_1x_4 + (1 - u_1\xi)b_2x_2x_4 - (1 + m)x_3,\\
\frac{dx_4}{d\tau} &= (1 - u_1\xi)(1 - p)b_1x_1x_4 + (1 - k)x_3 - \left(d_1 - \frac{d_2x_4}{c + bx_4}\right)x_4 - mx_4,
\end{aligned} \tag{2.3}$$

where we have success in reducing the dimension of system (2.1) into four dimensions and the number of parameters from 13 into 11 parameters.

2.2.2. TB-free equilibrium point and the reproduction number

There are two types of equilibrium points for our TB model in (2.3). The first equilibrium point is the TB-free equilibrium point where TB is extinct from the population, and the second is the TB-endemic equilibrium point where TB persists in the population (which will be discussed in the next section). The TB-free equilibrium point is given by:

$$\mathcal{E}_0 = (x_1^0, x_2^0, x_3^0, x_4^0) = \left(\frac{e + m}{e + m + u_2}, \frac{u_2}{e + m + u_2}, 0, 0\right). \tag{2.4}$$

The next significant calculation that we present is the computation of the respected reproduction number of system (2.3), indicated by $\mathcal{R}_c$. This reproduction number indicates the anticipated number of secondary tuberculosis cases resulting from one primary case during a single infection period, assuming the implementation of control measures in a wholly susceptible population. In many epidemic models, the reproduction number becomes the threshold to decide whether a disease would endure or become extinct. The predominant outcome is that diseases may vanish from the population if this threshold is below one. The reproduction number of system (2.3) is stated in the following theorem:

**Theorem 1.** *The reproduction number ($\mathcal{R}_c$) of non-dimensionalized TB model in system* (2.3) *is given by*

$$\mathcal{R}_c = \frac{(1-u_1\xi)(((1-p)m+1-kp)(e+m)b_1+b_2u_2(1-k))}{(e+m+u_2)(1+m)(d_1+m)}. \tag{2.5}$$

*Proof.* The proof is using the next-generation matrix method [27]. First, we evaluate the Jacobian matrix of infected compartments $(L, I)$ of system (2.3) on $\mathcal{E}_0$, which yield:

$$\mathbf{J} = \begin{bmatrix} -(1+m) & \frac{(1-u_1\xi)pb_1(e+m)}{(e+m+u_2)} + \frac{(1-u_1\xi)b_2u_2}{(e+m+u_2)} \\ (1-k) & \frac{(1-u_1\xi)(1-p)b_1(e+m)}{(e+m+u_2)} - (d_1+m) \end{bmatrix}.$$

Decompose $\mathbf{J}$ into transition ($\Sigma$) and transmission ($T$) matrices, where $\mathbf{J} = \Sigma + \mathbf{T}$, gives

$$\mathbf{T} = \begin{bmatrix} 0 & \frac{(1-u_1\xi)pb_1(e+m)}{e+m+u_2} + \frac{(1-u_1\xi)b_2u_2}{e+m+u_2} \\ 0 & \frac{(1-u_1\xi)(1-p)b_1(e+m)}{e+m+u_2} \end{bmatrix},$$

$$\Sigma = \begin{bmatrix} -(1+m) & 0 \\ (1-k) & -(d_1+m) \end{bmatrix}.$$

Hence, the next-generation matrix is given by

$$\begin{aligned} \mathbf{K} &= -\mathbf{T}\Sigma^{-1}, \\ &= -\begin{bmatrix} 0 & \frac{(1-u_1\xi)pb_1(e+m)}{e+m+u_2} + \frac{(1-u_1\xi)b_2u_2}{e+m+u_2} \\ 0 & \frac{(1-u_1\xi)(1-p)b_1(e+m)}{e+m+u_2} \end{bmatrix} \begin{bmatrix} -(1+m) & 0 \\ (1-k) & -(d_1+m) \end{bmatrix}^{-1}, \\ &= -\begin{bmatrix} 0 & \frac{(1-u_1\xi)pb_1(e+m)}{e+m+u_2} + \frac{(1-u_1\xi)b_2u_2}{e+m+u_2} \\ 0 & \frac{(1-u_1\xi)(1-p)b_1(e+m)}{e+m+u_2} \end{bmatrix} \begin{bmatrix} -\frac{1}{(1+m)} & 0 \\ \frac{k-1}{((1+m)(d_1+m))} & -\frac{1}{(d_1+m)} \end{bmatrix}, \\ &= \begin{bmatrix} \frac{(1-k)(pb_1(e+m)+b_2u_2)(1-u_1\xi)}{((e+m+u_2)(1+m)(d_1+m))} & \frac{(1-u_1\xi)(pb_1(e+m)+b_2u_2)}{((e+m+u_2)(d_1+m))} \\ \frac{(1-u_1\xi)(1-p)b_1(e+m)(1-k)}{((e+m+u_2)(1+m)(d_1+m))} & \frac{(1-u_1\xi)(1-p)b_1(e+m)}{((e+m+u_2)(d_1+m))} \end{bmatrix}. \end{aligned}$$

Therefore, the control reproduction number is given by the spectral radius of $\mathbf{K}$ is given by

$$\mathcal{R}_c = \frac{(1-u_1\xi)(((1-p)m+1-kp)(e+m)b_1+b_2u_2(1-k))}{(e+m+u_2)(1+m)(d_1+m)}.$$

From the formulation of $\mathcal{R}_c$, we may define the expression of the reproduction number when no control applies. We name this special case of $\mathcal{R}_c$ where $u_1 = u_2 = 0$ as the basic reproduction number. The expression of $\mathcal{R}_0$ is $\frac{((1-p)m+1-kp)b_1}{(e+m)(d_1+m)}$. From this expression, we derive the subsequent corollary.

**Corollary 1.** *The basic reproduction number (where $u_1 = u_2 = 0$) of TB model in* (2.3) *is given by:*

$$\mathcal{R}_0 = \frac{((1-p)m+1-kp)b_1}{(e+m)(d_1+m)}, \tag{2.6}$$

*where $\mathcal{R}_c < \mathcal{R}_0$ always satisfies for all $u_1 \in (0, 1]$ and $u_2 > 0$.*

The basic reproduction number $\mathcal{R}_0$ represents the average number of secondary infections of TB in our case, which is generated by one infectious individual in a completely susceptible population and in the absence of any control measures. On the other hand, $\mathcal{R}_c$ accounts for interventions such as media campaign and mask use intervention. Both this threshold helps to assess whether implemented strategies are sufficient to bring the reproduction number below unity, thereby ensuring TB elimination.

### 2.2.3. Stability of TB-free equilibrium point

To analyze the local stability of the TB-free equilibrium point, we use a linearization approach of system (2.3) on TB-free equilibrium point which gives:

$$\mathbf{J}_{\mathcal{E}_0} = \begin{bmatrix} -(m+u_2) & e & 0 & -\frac{(1-u_1\xi)b_1(e+m)}{(e+m+u_2)} \\ u_2 & -(e+m) & 0 & -\frac{(1-u_1\xi)b_2u_2}{(e+m+u_2)} \\ 0 & 0 & -(1+m) & \frac{(1-u_1\xi)pb_1(e+m)}{(e+m+u_2)} + \frac{(1-u_1\xi)b_2u_2}{(e+m+u_2)} \\ 0 & 0 & (1-k) & \frac{(1-u_1\xi)(1-p)b_1(e+m)}{(e+m+u_2)} - (d_1+m) \end{bmatrix}.$$

The characteristic polynomial of $\mathbf{J}_{\mathcal{E}_0}$ is given by

$$g(\lambda) = (\lambda+m)(\lambda+(m+e+u_2))(\lambda^2+b_1\lambda+b_0) = 0,$$

where $b_1 = (2m+d_1+1) - \dfrac{(1-u_1\xi)(e+m)(1-p)b_1}{(e+m+u_2)}$ and $b_0 = (1+m)(d_1+m)(1-\mathcal{R}_c)$. TB-free equilibrium point $\mathcal{E}_0$ is locally asymptotically stable if all real part of the eigenvalues of $\mathbf{J}_{\mathcal{E}_0}$ are negative. From the expression of $g(\lambda)$, we have two explicit negative eigenvalues, i.e., $\lambda_1 = -m$ and $\lambda_2 = -(m+e+u_2)$. The other two eigenvalues, $\lambda_3$ and $\lambda_4$, are taken from the roots of $\lambda^2 + b_1\lambda + b_0 = 0$. Hence, $Re\{\lambda_3, \lambda_4\} < 0$ if $\lambda_3\lambda_4 > 0$ and $\lambda_3 + \lambda_4 < 0$. Since $\lambda_3\lambda_4 = b_0$, then $b_0 > 0 \iff \mathcal{R}_c < 1$. On the other hand, $\lambda_3 + \lambda_4 = -b_1 < 0 \iff b_1 > 0 \iff \mathcal{R}_1 = \dfrac{(1-u_1\xi)(e+m)(1-p)b_1}{(e+m+u_2)(2m+d_1+1)} < 1$. From direct calculation, it can be shown that $\mathcal{R}_1 < \mathcal{R}_c$. Therefore, the TB-free equilibrium point is locally asymptotically stable if $\mathcal{R}_c < 1$. This result stated in the following theorem.

**Theorem 2.** *The TB-free equilibrium point $\mathcal{E}_0$ is locally asymptotically stable if $\mathcal{R}_c < 1$ and unstable if $\mathcal{R}_c > 1$.*

### 2.2.4. The endemic equilibrium point

The second equilibrium point of system (2.3) is the TB-endemic equilibrium point and is given in the form of:

$$\mathcal{E}_1 = (x_1^*, x_2^*, x_3^*, x_4^*), \tag{2.7}$$

where

$$x_1^* = \frac{m(b_2x_4(1-u_1\xi)+e+m)}{b_1b_2(1-u_1\xi)^2x_4^2 + x_4((b_1+b_2)m+eb_1+b_2u_2)(1-u_1\xi)+m(e+m+u_2)},$$

$$x_2^* = \frac{mu_2}{b_1b_2(1-u_1\xi)^2x_4^2 + x_4((b_1+b_2)m+eb_1+b_2u_2)(1-u_1\xi)+m(e+m+u_2)},$$

$$x_3^* = \frac{mx_4(1-u_1\xi)(p(b_2(1-u_1\xi)x_4+e+m)b_1+b_2u_2)}{(1+m)(m^2+(x_4(b_1+b_2)(1-u_1\xi)+e+u_2)m+(1-u_1\xi)x_4(b_1b_2(1-u_1\xi)x_4eb_1+b_2u_2))}.$$

and $x_4^*$ is the positive roots from the following polynomials:

$$f(x_4) = a_3x_4^3 + a_2x_4^2 + a_1x_4 + a_0 = 0, \tag{2.8}$$

with

$$\begin{aligned}
a_3 &= b_1b_2(1-u_1\xi)^2(1+m)((d_1+m)b-d_2),\\
a_2 &= ((1+m)(d_1+m)c-((1-p)m+1-kp)bm)b_1b_2(1-u_1\xi)^2+(1+m)\\
&\quad ((b_1+b_2)m+eb_1+b_2u_2)((m+d_1)b-d_2)(1-u_1\xi),\\
a_1 &= -cmb_1b_2(1-u_1\xi)^2((1-p)m+1-kp)+((1+m)(m+u_2)(d_1+m)c-\\
&\quad ((e+m)((1-p)m+1-kp)b_1-b_2u_2(1-k))mb)(1-u_1\xi)-md_2(1+m)\\
&\quad (e+m+u_2)+m(1+m)(e+m+u_2)(d_1+m)b\\
a_0 &= cm(1+m)(d_1+m)(e+m+u_2)(1-\mathcal{R}_c).
\end{aligned}$$

Since $bd_1 > d_2$, then $a_3$ is always positive. Since $a_3$ is always positive, and $a_0 < 0 \iff \mathcal{R}_c > 1$, then we have the following theorem.

**Theorem 3.** *There is always exist an endemic equilibrium point $\mathcal{E}_1$ whenever $\mathcal{R}_c > 1$.*

Polynomial $f(x_4)$ is a three degree polynomial. It is possible to have more than one endemic equilibrium point for system (2.3). Hence, we use the Descartes rules of sign to analyze this possibility further. The results is given in Table 2.

**Table 2.** Possible number of positive roots of polynomial (2.8).

| Case | $a_3$ | $a_2$ | $a_1$ | $a_0$ | $\mathcal{R}_c$ | Possible number of positive roots |
|---|---|---|---|---|---|---|
| 1 | + | + | + | + | $\mathcal{R}_c < 1$ | 0 |
| 2 | + | + | - | + | $\mathcal{R}_c < 1$ | 0 or 2 |
| 3 | + | - | + | + | $\mathcal{R}_c < 1$ | 0 or 2 |
| 4 | + | - | - | + | $\mathcal{R}_c < 1$ | 0 or 2 |
| 5 | + | + | + | - | $\mathcal{R}_c > 1$ | 1 |
| 6 | + | + | - | - | $\mathcal{R}_c > 1$ | 1 |
| 7 | + | - | + | - | $\mathcal{R}_c > 1$ | 1 or 3 |
| 8 | + | - | - | - | $\mathcal{R}_c > 1$ | 1 |

From Table 2, it can be seen that it is still possible to have two endemic equilibrium points for the case of $\mathcal{R}_c < 1$ (cases 2–4). Furthermore, it is also possible to have three endemic equilibrium points when $\mathcal{R}_c > 1$ (case 7). We use a gradient analysis on the bifurcation point $\mathcal{R}_c = 1$ to determine a condition when we may have an endemic equilibrium point when $\mathcal{R}_c < 1$. Hence, we need to determine the sign of $\dfrac{\partial x_4}{\partial \mathcal{R}_c}$ at $\mathcal{R}_c = 1, x_4 = 0$. If it is negative, then we will have an endemic equilibrium point for some interval values of $\mathcal{R}_c < 1$. To do the analysis, first we rewrite the polynomial $f(x_4)$ as a function

dependent on $\mathcal{R}_c$. Let $b_1(\mathcal{R}_c)$ be the bifurcation parameter. From the expression of $\mathcal{R}_c$ in (2.5), $b_1$ as a function of $\mathcal{R}_c$ is given by:

$$b_1^* = \mathcal{R}_c \frac{(e+m+u_2)(1+m)(d_1+m) - (1-u_1\xi)(b_2u_2(1-k))}{(1-u_1\xi)((1-p)m+1-kp)(e+m)}.$$

Substituting this $b_1^*$ into $f(x_4)$ yields:

$$f^*(x_4) = a_3(\mathcal{R}_c)(x_4)^3 + a_2(\mathcal{R}_c)(x_4)^2 + a_1(\mathcal{R}_c)x_4 + a_0(\mathcal{R}_c) = 0.$$

Taking the implicit derivatives of $f(x_4)$ with respect to $\mathcal{R}_c$ at $\mathcal{R}_c = 1$ and $x_4 = 0$,solving it with respect to $\dfrac{\partial x_4}{\partial \mathcal{R}_c}$ gives:

$$\frac{\partial x_4}{\partial \mathcal{R}_c} = -\frac{\partial a_0(\mathcal{R}_c)}{\partial \mathcal{R}_c}\left(\frac{1}{a_1(\mathcal{R}_c=1)}\right),$$

where $\dfrac{\partial a_0(\mathcal{R}_c)}{\partial \mathcal{R}_c} = -cm(e+m+u_2)(1+m)(d_1+m)$ and $\left(\dfrac{1}{a_1(\mathcal{R}_c=1)}\right) = \dfrac{c(P+Q+R)-S}{((1-p)m+1-kp)(e+m)}$ with

$$\begin{aligned}
P &= b_2^2(1-u_1\xi)^2u_2m(1-k)((1-p)m+1-kp),\\
Q &= u_2b_2(1-u_1\xi)(1+m)(d_1+m)((1-p)(k+m)e-(1-k)m),\\
R &= (1+m)^2(d_1+m)^2(e+m)(e+m+u_2),\\
S &= (1+m)(e+m)(e+m+u_2)((1-p)m+1-kp)md_2.
\end{aligned}$$

Since $\dfrac{\partial a_0(\mathcal{R}_c)}{\partial \mathcal{R}_c}$ is always negative, then the sign of $\frac{\partial x_4}{\partial \mathcal{R}_c}$ at $\mathcal{R}_c = 1, x_4 = 0$ is dependent on the sign of $a_1$ at $\mathcal{R}_c = 1$. From direct calculation, we have

$$\frac{\partial x_4}{\partial \mathcal{R}_c} < 0 \iff c < c^* = \frac{S}{P+Q+R}.$$

With these results and combining them with the result from Table 2, we have the following theorem.

**Theorem 4.** *Let* $c^* = \dfrac{S}{P+Q+R}$ *where* $P = b_2^2(1-u_1\xi)^2u_2m(1-k)((1-p)m+1-kp)$, $Q = u_2b_2(1-u_1\xi)(1+m)(d_1+m)((1-p)(k+m)e-(1-k)m)$, $R = (1+m)^2(d_1+m)^2(e+m)(e+m+u_2)$, $S = (1+m)(e+m)(e+m+u_2)((1-p)m+1-kp)md_2$, *and* $\mathcal{R}_c^*$ *is* $\mathcal{R}_c$ *that satisfies the discriminant of* $f(x_4)$ *given by* $a_2^2a_1^2$–$4a_3a_1^3$–$4a_2^3a_0$–$27a_3^2a_0^2 + 18a_3a_2a_1a_0$ *equal to zero. If* $c < c^*$, *then the TB model in* (2.3) *has two endemic equilibrium points for* $\mathcal{R}_c^* < \mathcal{R}_c < 1$.

For a specific case when $\mathcal{R}_c = 1$, it is possible to have two endemic equilibrium points. If $\mathcal{R}_c = 1$, then we have $a_0 = 0$, which gives one zero roots of polynomial $f(x_4)$. The other two roots are taken from the following polynomial:

$$f^\dagger(x_4) = a_3(\mathcal{R}_c)x_4^2 + a_2(\mathcal{R}_c)x_4 + a_1(\mathcal{R}_c) = 0.$$

We have two positive roots that satisfy $f^\dagger(x_4) = 0$ if $a_1 > 0 \iff c > c^*, a_2 < 0$, and $a_2^2 - 4a_3a_1 > 0$. With this result, we will have two turning point of $f^*(x_4)$. One of them appears on some specific value at $\mathcal{R}_c > 1$, and the other one is when $\mathcal{R}_c < 1$. Hence, it is possible to have three endemic equilibrium points for some interval of $\mathcal{R}_c > 1$ if $a_1 > 0 \iff c > c^*, a_2 < 0$, and $a_2^2 - 4a_3a_1 > 0$. We conclude this result with the following theorem.

**Theorem 5.** *Let $\mathcal{R}_c^1$ and $\mathcal{R}_c^2$ are the turning point of $f^*(x_4)$ that satisfies $\frac{\partial f^*(x_4)}{\partial \mathcal{R}_c} = 0$ where $\mathcal{R}_c^2 > \mathcal{R}_c^1$. If $c > c^*, a_2 < 0$, and $a_2^2 - 4a_3a_1 > 0$, then the tuberculosis model in* (2.3) *has:*

*1) Three endemic equilibrium points in $1 < \mathcal{R}_c < \mathcal{R}_c^2$,*

*2) Two endemic equilibrium points in $\mathcal{R}_c^1 < \mathcal{R}_c < 1$.*

To close this section, we conclude our calculation on the possible appearance of the endemic equilibrium point as follows:

1) There is always at least one endemic equilibrium point if $\mathcal{R}_c > 1$.

2) If $c < c^*$, then there exist two endemic equilibrium points for $\mathcal{R}_c^* < \mathcal{R}_c < 1$.

3) It is possible to have three endemic equilibrium points when $\mathcal{R}_c > 1$ and two endemic equilibrium points when $\mathcal{R}_c < 1$ if $c > c^*, a_2 < 0$, and $a_2^2 - 4a_3a_1 > 0$.

The calculation suggests a scenario where the traditional public health criterion that a basic reproduction number below 1 ensures the eradication of TB might not hold true. In our proposed model, this is due to factors such as the saturated treatment effect. A saturated treatment effect is observed when the maximum benefit of TB treatment is achieved, and further treatment attempts result in reduced benefits. This can occur as a result of constrained healthcare resources. This factor imply that even with effective treatments reducing the transmission rate, TB might persist in the population, necessitating a more comprehensive public health approach that addresses these complexities.

## 3. Existence of backward bifurcation

To analyze the existence of backward bifurcation at $\mathcal{R}_c = 1$, we apply the Castillo Chavez and Song bifurcation theorem [28]. This theorem has been implemented widely by many authors on their epidemic models to analyze type of bifurcation that appears in $\mathcal{R}_0 = 1$ (or $\mathcal{R}_c = 1$). See [29–35] for more examples. First, let $\frac{dx_i}{dt}$ in Eq (2.3) as $f_i$ for $i = 1, 2, 3, 4$. Next, we choose $b_1$ as the bifurcation parameter, where $b_1^*$ is the critical value obtained from $\mathcal{R}_c = 1$. Linearization of system (2.3) around $\mathcal{E}_0$ and $b_1^*$ gives:

$$\mathcal{J}(\mathcal{E}_0, b_1^*) = \begin{bmatrix} -m-u_2 & e & 0 & C1 \\ u_2 & -e-m & 0 & \frac{b_2u_2(\xi u_1-1)}{e+m+u_2} \\ 0 & 0 & -1-m & C2 \\ 0 & 0 & 1-k & C3 \end{bmatrix},$$

where :

$$\begin{aligned} C1 &= \frac{b_2u_2\left(1-\xi u_1\right)k + m^3 + \left(e+d_1+u_2+1\right)m^2 + \left(\left(d_1+1\right)u_2 + \left(e+1\right)d_1 + e\right)m + \left(\xi u_1b_2 - b_2 + d_1\right)u_2 + ed_1}{\left(e+m+u_2\right)\left(kp-1+\left(p-1\right)m\right)}, \\ C2 &= -\frac{\left(\left(m^2 + \left(e+d_1+u_2\right)m + \left(\xi u_1b_2 - b_2 + d_1\right)u_2 + ed_1\right)p - b_2u_2\left(\xi u_1 - 1\right)\right)\left(1+m\right)}{\left(kp+mp-m-1\right)\left(e+m+u_2\right)}, \\ C3 &= -\frac{\left(\left(\left(\xi u_1b_2 + m - b_2 + d_1\right)u_2 + \left(d_1+m\right)\left(e+m\right)\right)p - b_2u_2\left(\xi u_1 - 1\right)\right)\left(k-1\right)}{\left(kp+mp-m-1\right)\left(e+m+u_2\right)}. \end{aligned}$$

The eigenvalues of $\mathcal{J}(\mathcal{E}_0, b_1^*)$ are $\lambda_1 = 0, \lambda_2 = -m, \lambda_3 = -(e + m + u_2)$, and

$$\lambda_4 = -\frac{(1 - u_1\xi)b_2u_2(1 - p)(1 - k) + (e + m + u_2)\left((1 - p)m^2 + 2(1 - kp) + (1 - k)pd_1 + 1 - kp\right)}{((1 - p)m + 1 - kp)(e + m + u_2)}.$$

It can be seen that $\mathcal{J}(\mathcal{E}_0, b_1^*)$ has a simple zero eigenvalue, while the other three are negative. Hence, the Center Manifold Theorem can be applied, and the Castillo–Song bifurcation theorem ensures that a local bifurcation occurs at $b_1 = b_1^*$.

Next, we compute the left eigenvector of $\mathcal{J}(\mathcal{E}_0, b_1^*)$ corresponding to the zero eigenvalue $\lambda_1 = 0$, denoted by $v$. Through direct calculation, we obtain:

$$v = \left\{v_1 = 0, v_2 = 0, v_3 = \frac{1 - k}{1 + m}, v_4 = 1\right\}.$$

Similarly, we determine the corresponding right eigenvector associated with $\lambda_1 = 0$, denoted by $w$, and find $w = \{w_1, w_2, w_3, w_4\}$:

$$\begin{aligned}
w_1 &= -\frac{b_2u_2(1 - u_1\xi)((1 - p)(k + m)e + m(1 - k))}{(e + m + u_2)^2((1 - p)m + 1 - kp)m} \\
&\quad + \frac{(1 + m)(e + m)(e + m + u_2)(d_1 + m)}{(e + m + u_2)^2((1 - p)m + 1 - kp)m}, \\
w_2 &= -\frac{u_2((1 - p)m^2 + ((1 - p)u_2 + 1 - kp)m + ku_2(1 - p))(1 - u_1\xi)b_1}{(e + m + u_2)^2((1 - p)m + 1 - kp)m} \\
&\quad - \frac{w_4u_2(1 + m)(d_1 + m)}{(e + m + u_2)((1 - p)m + 1 - kp)m}, \\
w_3 &= \frac{b_2u_2(1 - p)(1 - u_1\xi) + p(e + m + u_2)(d_1 + m)}{(e + m + u_2)(1 + m)(d_1 + m)}, \\
w_4 &= 1.
\end{aligned}$$

To determine the type of bifurcation that arise at $\mathcal{R}_c = 1$, we substitute the above result into the following formula:

$$\mathscr{A} = \sum_{k,i,j=1}^{4} v_k w_i w_j \frac{\partial^2 f_k}{\partial x_i \partial x_j}(\mathcal{E}_0, b_1^*), \qquad \mathscr{B} = \sum_{k,i=1}^{4} v_k w_i \frac{\partial^2 f_k}{\partial x_i \partial \beta}(\mathcal{E}_0, b_1^*).$$

By direct calculation, we have:

$$\begin{aligned}
\mathscr{A} &= 2p\,(-\xi u_1 + 1)\,b_1 v_3 w_1 w_4 + 2\,(-\xi u_1 + 1)\,b_2 v_3 w_2 w_4 + 2\,(1 - p)\,(-\xi u_1 + 1)\,b_1 v_4 w_1 w_4 + \frac{2d_2 v_4\, {w_4}^2}{c}, \\
\mathscr{B} &= \frac{(1 - \xi u_1)\,((1 - p)m + (1 - pk))}{(e + m + u_2)\,(1 + m)} > 0.
\end{aligned}$$

It can be seen that $\mathscr{A}$ could be positive or negative, depending on the combination of parameter values of the model. Based on this calculation, we state the result in the following theorem.

**Theorem 6.** *TB model in* (2.3) *undergoes:*

*1) Forward bifurcation at* $\mathcal{R}_c = 1$ *if* $\mathscr{A} < 0$*, and*

*2) Backward bifurcation at* $\mathcal{R}_c = 1$ *if* $\mathscr{A} > 0$*.*

In conclusion, determining whether a forward or backward bifurcation occurs at the critical threshold $\mathcal{R}_c = 1$ is crucial, as it directly influences the long-term behavior of the system. A forward bifurcation implies that reducing $\mathcal{R}_c$ below unity is sufficient for disease elimination, whereas a backward bifurcation indicates the potential for disease persistence even when $\mathcal{R}_c < 1$, thereby necessitating stronger or combined control strategies. More discussions will be provided in the numerical experiment section.

## 4. Investigation of Hopf bifurcation

To investigate the potential emergence of oscillatory behavior near the endemic equilibrium point $\mathcal{E}_1$, here we analyze the occurrence of Hopf bifurcation from our non-dimensionalized model in system (2.3). This type of bifurcation arises when a pair of complex conjugate eigenvalues of the Jacobian matrix of system (2.3) evaluated in $\mathcal{E}_1$ crosses the imaginary axis as the bifurcation parameter varies. For our analysis, we choose the infection parameter $b_1$ as the bifurcation parameter.

First, we calculate the Jacobian matrix of system (2.3) which is evaluated in $\mathcal{E}_1$. By direct calculation, we have

$$\mathcal{J}(\mathcal{E}_1) = \left[\begin{array}{c|c} A & B \\ \hline C & D \end{array}\right], \tag{4.1}$$

where

$$A = \begin{bmatrix} -m - p(1-u_1\xi)b_1x_4^* - (1-p)(1-u_1\xi)b_1x_4^* - u_2 & e \\ u_2 & -(1-u_1\xi)b_2x_4^* - e - m \end{bmatrix},$$

$$B = \begin{bmatrix} 0 & -p(1-u_1\xi)b_1x_1^* - (1-p)(1-u_1\xi)b_1x_1^* \\ 0 & -(1-u_1\xi)b_2x_2^* \end{bmatrix},$$

$$C = \begin{bmatrix} p(1-u_1\xi)b_1x_4^* & (1-u_1\xi)b_2x_4^* \\ (1-p)(1-u_1\xi)b_1x_4^* & 0 \end{bmatrix},$$

$$D = \begin{bmatrix} -1-m & p(1-u_1\xi)b_1x_1^* + (1-u_1\xi)b_2x_2^* \\ 1-k & (1-p)(1-u_1\xi)b_1x_1^* - \left(-\dfrac{d_2}{bx_4^*+c} + \dfrac{d_2x_4^*b}{(bx_4^*+c)^2}\right)x_4^* - d_1 + \dfrac{d_2x_4^*}{bx_4^*+c} - m \end{bmatrix}$$

As mentioned earlier, we choose $b_1$ as the bifurcation parameter. Accordingly, the characteristic polynomial associated with the Jacobian matrix $\mathcal{J}(\mathcal{E}_1)$, used to determine the eigenvalues, is given by

$$P(b_1, \lambda) = \lambda^4 + c_3(b_1)\lambda^3 + c_2(b_1)\lambda^2 + c_1(b_1)\lambda + c_0(b_1) = 0, \tag{4.2}$$

where the coefficients $c_i(b_1)$ are too complex to be presented explicitly in this article. According to [36], a Hopf bifurcation may occur only if the following conditions are satisfied:

(A) All coefficients of the characteristic polynomial in (4.2) are positive, i.e., $c_i(b_1^*) > 0$ for $i = 0, 1, 2, 3$,

(B) The Hurwitz determinant $\Delta_2(b_1^*)$ is positive, and $\Delta_3(b_1^*) = 0$,

(C) The transversality condition holds, i.e., $\dfrac{d\lambda}{db_1}(b_1^*) \neq 0$, where $\lambda$ denotes an eigenvalue of the polynomial in (4.2).

To verify the existence of a Hopf bifurcation, we examine whether the system satisfies all conditions listed above. First, we confirm that all coefficients of the characteristic polynomial $P(b_1, \lambda)$ are positive at a critical value $b_1 = b_1^*$, i.e., $c_i(b_1^*) > 0$ for $i = 0, 1, 2, 3$, ensuring that the system is initially in a stable configuration. Next, we locate the critical value $b_1^*$ for which the third Hurwitz determinant vanishes, i.e., $\Delta_3(b_1^*) = c_3c_2c_1 - c_3^2c_0 - c_1^2 = 0$, signifying the potential emergence of a pair of purely imaginary eigenvalues. Furthermore, we also compute the other Hurwitz determinant $\Delta_2(b_1) = c_3(b_1)c_2(b_1) - c_1(b_1)$ and show that $\Delta_2(b_1^*) > 0$, indicating local stability prior to bifurcation. Finally, instead of verifying the full derivative $\frac{d\lambda}{db_1}(b_1^*)$, we check the transversality condition by confirming that the real part of the eigenvalue crosses zero with nonzero speed, i.e.,

$$\left.\frac{d\,\mathrm{Re}(\lambda)}{db_1}\right|_{b_1=b_1^*} \neq 0.$$

This condition ensures that the eigenvalues move transversely across the imaginary axis. To show this last condition, differentiating (4.2) with respect to $b_1$ gives

$$\frac{dP}{db_1} = 4\lambda^3\frac{d\lambda}{db_1} + \frac{dc_3(b_1)}{db_1}\lambda^3 + 3c_3(b_1)\lambda^2\frac{d\lambda}{db_1} + \frac{dc_2(b_1)}{db_1}\lambda^2 + 2c_2(b_1)\lambda\frac{d\lambda}{db_1} + \frac{dc_1(b_1)}{db_1}\lambda + c_1(b_1)\frac{d\lambda}{db_1} + \frac{dc_0(b_1)}{db_1} = 0.$$

Solving the above equations with respect to $\frac{d\lambda}{db_1}$, we get

$$\frac{d\lambda}{db_1} = -\frac{\frac{dc_3(b_1)}{db_1}\lambda^3 + \frac{dc_2(b_1)}{db_1}\lambda^2 + \frac{dc_1(b_1)}{db_1}\lambda + \frac{dc_0(b_1)}{db_1}}{4\lambda^3 + 3c_3(b_1)\lambda^2 + 2c_2(b_1)\lambda + c_1(b_1)}.$$

Substituting $\lambda = i\omega$ and $b_1 = b_1^*$, we have the real part of $\frac{d\lambda}{db_1}$, which is given by

$$\left.\frac{d\,\mathrm{Re}(\lambda)}{db_1}\right|_{x=i\omega, b_1=b_1^*} = \frac{\left(\frac{dc_0}{db_1} - \frac{dc_2}{db_1}\omega^2\right)\left(c_1 - 3c_3\omega^2\right) + \left(\frac{dc_1}{db_1}\omega - \frac{dc_3}{db_1}\omega^3\right)\left(2c_2\omega - 4\omega^3\right)}{(c_1 - 3c_3\omega^2)^2 + (2c_2\omega - 4\omega^3)^2},$$

while the imaginary part is given by

$$\left.\frac{d\,\mathrm{Im}(\lambda)}{db_1}\right|_{x=i\omega, b_1=b_1^*} = \frac{\left(\frac{dc_1}{db_1}\omega - \frac{dc_3}{db_1}\omega^3\right)\left(c_1 - 3c_3(b_1)\omega^2\right) - \left(\frac{dc_0}{db_1} - \frac{dc_2}{db_1}\omega^2\right)\left(2c_2\omega - 4\omega^3\right)}{(c_1 - 3c_3\omega^2)^2 + (2c_2\omega - 4\omega^3)^2}.$$

Therefore, we have that $\left.\dfrac{d\,\mathrm{Re}(\lambda)}{db_1}\right|_{x=i\omega, b_1=b_1^*} \neq 0$ if

$$\left(\frac{dc_0}{db_1} - \frac{dc_2}{db_1}\omega^2\right)\left(c_1 - 3c_3\omega^2\right) + \left(\frac{dc_1}{db_1}\omega - \frac{dc_3}{db_1}\omega^3\right)\left(2c_2\omega - 4\omega^3\right) \neq 0.$$

This result is summarized in the following theorem.

**Theorem 7.** *The TB model described in* (2.3) *undergoes a Hopf bifurcation from the endemic equilibrium point* $\mathcal{E}_1$ *at the critical parameter value* $b_1 = b_1^*$ *if the characteristic polynomial coefficients satisfy the following conditions:*

- $c_3, c_2, c_1, c_0 > 0$,
- $c_3c_2 - c_1 > 0$,
- $c_3c_2c_1 - c_3^2c_0 - c_1^2 = 0$,

*along with the transversality condition:*

$$\left(\frac{dc_0}{db_1} - \frac{dc_2}{db_1}\omega^2\right)\left(c_1 - 3c_3\omega^2\right) + \left(\frac{dc_1}{db_1}\omega - \frac{dc_3}{db_1}\omega^3\right)\left(2c_2\omega - 4\omega^3\right) \neq 0,$$

*where* $\omega \neq 0$ *is the imaginary part of the purely imaginary pair of eigenvalues at* $b_1 = b_1^*$, *and* $c_i$ *for* $i = 0, 1, 2, 3$ *is the coefficient of polynomial* (4.2).

## 5. Numerical experiments

In the preceding section, we formulated our TB model taking into account variables such as constrained treatment resources, reinfection, public knowledge, and the slow-fast progression of infection. The model is introduced in system (2.1) and then simplified to system (2.3) by making the assumption of a constant total population. In this section, we perform numerical experiments to gain a deeper understanding of the qualitative dynamics of our TB model, with a specific emphasis on examining the effects of media campaigns and restricted treatment facilities on strategies for preventing TB. Initially, we determine the parameters of our model by utilizing incidence data per 100,000 inhabitants in Indonesia spanning 2000 to 2020. The data were acquired from [37] and are readily available to readers under the license 4.0. With these predicted parameter values, we perform numerical experiments that involve sensitivity analysis and autonomous simulations to see the evolution of our model. These tests illustrate the biological consequences of our study, as mentioned in Section 2.2.4.

### *5.1. Parameter estimation*

In this section, we calculate our parameter values by utilizing the *fmincon* toolbox provided in Matlab. The data utilized to estimate the parameters is depicted by the red curve in Figure 2(a). This graph illustrates a declining trend in the number of new cases of tuberculosis in Indonesia per 100,000 individuals. Notwithstanding this decrease, it is imperative to predict the potential consequences in the imminent future, particularly in light of Indonesia's objective to eradicate TB by 2030. Precisely quantifying these factors will enhance our comprehension of the dynamics of TB transmission and control, and empower us to make well-informed forecasts regarding future trends. Our goal is to find the best initial conditions and parameters that will make sure the output of our model matches the patterns seen in the new incidence data shown in Figure 2. It is noteworthy that various authors have computed certain parameter values for their own models. It is important to remember that various epidemiological models can produce different optimal parameter values, although these variations may be minimal in certain instances. Our goal is to improve the dependability of our model in

forecasting trends and comprehending the dynamics of disease occurrence by precisely calculating these parameters.

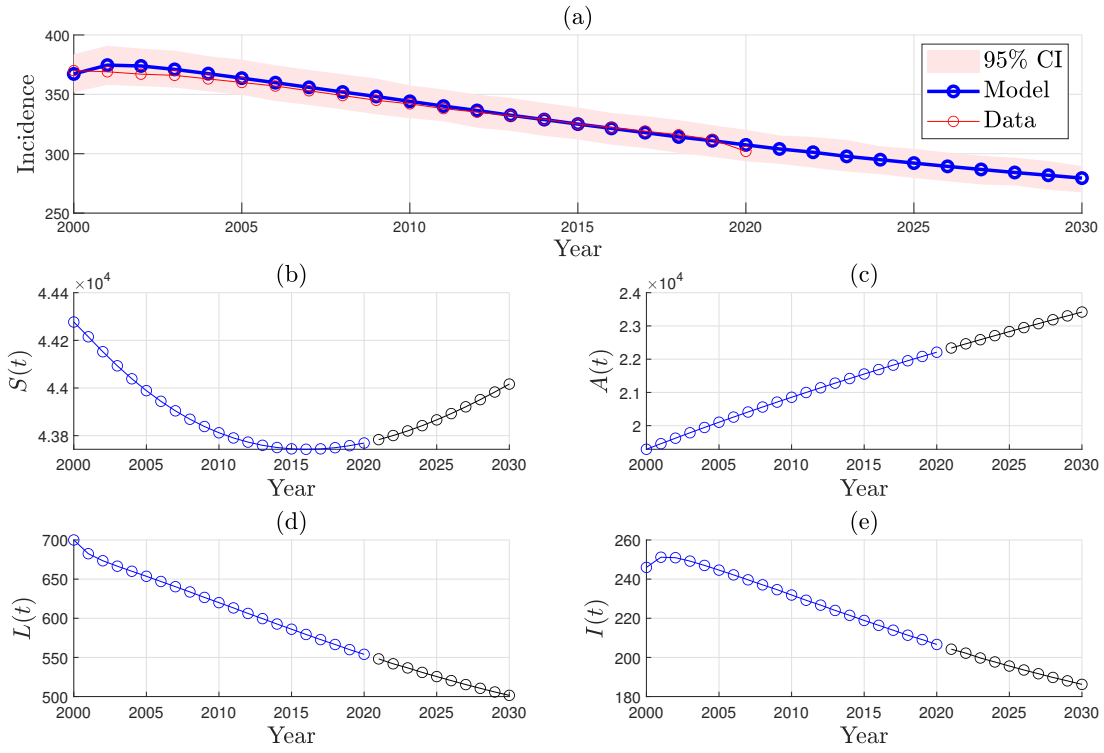


**Figure 2.** (a) Curve fitting results using new incidence data per 100,000 individuals in Indonesia. The black curve shows the forecasting results for 10 years onward, from 2021 until 2031. Panels (b) to (e) show the dynamics of $S(t)$, $A(t)$, $L(t)$, and $I(t)$, respectively.

As mentioned, the data available is the new incidence per 100,000 individuals. In our model, the new incidence data is represented by the following term:

$$\text{New incidence} = (1 - u_1\xi)(\beta_1 S + \beta_2 A)I,$$

where $\beta_2 \leq \beta_1$. Hence, we need to seek a best fit parameter:

$$\{\beta_1, \beta_2, u_1, \bar{u_2}, \xi, \eta, p, k, \alpha, \gamma_m, \gamma_0, b\},$$

and initial condition:

$$\{S(0), A(0), L(0), I(0), R(0)\},$$

such that the following cost function:

$$\mathcal{J} = \sum_{i=1}^{21} ((1 - u_1\xi)(\beta_1 S + \beta_2 A)I - \text{data})^2$$

can be minimized. Using the *fmincon* toolbox in Matlab, we find the best fit parameter values and initial condition, which gives the results in Figure 2(a) given by:

$$\beta_1 = 3.2 \times 10^{-5}, \beta_2 = 3.93 \times 10^{-6}, u_1 = 0, \bar{u_2} = 0.01, \xi = 0.56, \eta = 5.5295 \times 10^{-7},$$
$$p = 0.899, k = 0.373341, \alpha = 0.5, \gamma_m = 1, \gamma_0 = 9.9947 \times 10^{-5}, b = 10^{-4},$$
$$S(0) = 44277, A(0) = 19289, L(0) = 700, I(0) = 246, R(0) = 24282.$$

To quantify the uncertainty around the model predictions, we construct a 95% confidence interval (CI) for the model-generated incidence using a bootstrap-based approach with relative error. Using the data above, the dynamics of compartments $S$, $A$, $L$, and $I$ are presented in Figure 2, panels (b) to (e), respectively.

In panels (b) to (e) of Figure 2, we extend our simulation over the next 10 years to forecast the future of TB in Indonesia. The results indicate that with the current government programs, the number of new cases per 100,000 individuals may continue to decline but will not be completely eradicated by 2031. Therefore, more comprehensive interventions are required to accelerate the goal of TB elimination by 2031. In the next section, we continue our analysis by exploring the potential of face masks and media campaigns to enhance the chances of TB elimination in Indonesia.

### *5.2. Sensitivity analysis of $\mathcal{R}_c$*

#### 5.2.1. Global sensitivity analysis

**Table 3.** The numerical PRCC values and the corresponding $p$-values of the parameters of TB slow-fast progression model $\mathcal{R}_c$.

| Parameter | PRCC | P-value | Keep |
|---|---|---|---|
| $e$ | 0.004856344 | $8.787e^{-01}$ | FALSE |
| $m$ | 0.301509267 | $0.000e^{+00}$ | TRUE |
| $u_2$ | -0.235991030 | $4.019e^{-14}$ | TRUE |
| $d_1$ | -0.768972664 | $0.000e^{+00}$ | TRUE |
| $b_2$ | 0.104436076 | $9.853e^{-04}$ | TRUE |
| $k$ | -0.078726091 | $1.315e^{-02}$ | TRUE |
| $b_1$ | 0.725800659 | $0.000e^{+00}$ | TRUE |
| $p$ | -0.109847318 | $5.268e^{-04}$ | TRUE |
| $u_1$ | 0.032139141 | $3.122e^{-01}$ | FALSE |
| $\xi$ | 0.775143706 | $0.000e^{+00}$ | TRUE |

The sensitivity analysis of $\mathcal{R}_c$ is conducted to evaluate how changes in key parameters influence disease dynamics, especially regarding their effect on the spread of infection. To assess the sensitivity of the model's parameters, we employ a robust statistical approach that combines Latin Hypercube Sampling (LHS) with Partial Rank Correlation Coefficients (PRCC), as described in [38]. This technique is particularly effective in detecting monotonic nonlinear relationships between the model's inputs and its outcomes. With this approach, we calculate the PRCC values for each parameter along with their associated p-values. These values provide insight into the uncertainty within the dynamic model. The parameters with the highest absolute PRCC values and the lowest p-values are recognized

as the most influential in the model. The results obtained are presented in Table 3, while the PRCC plot is shown in Figure 3(a) in addition to the distribution of the $\mathcal{R}_c$ for 1000 runs given by Figure 3(b). Note that in Table 3, the "Keep" column indicates whether a parameter is statistically significant (TRUE, p-value $< 0.05$) and should be retained in the model or not significant (FALSE) and potentially may be excluded from further analysis.

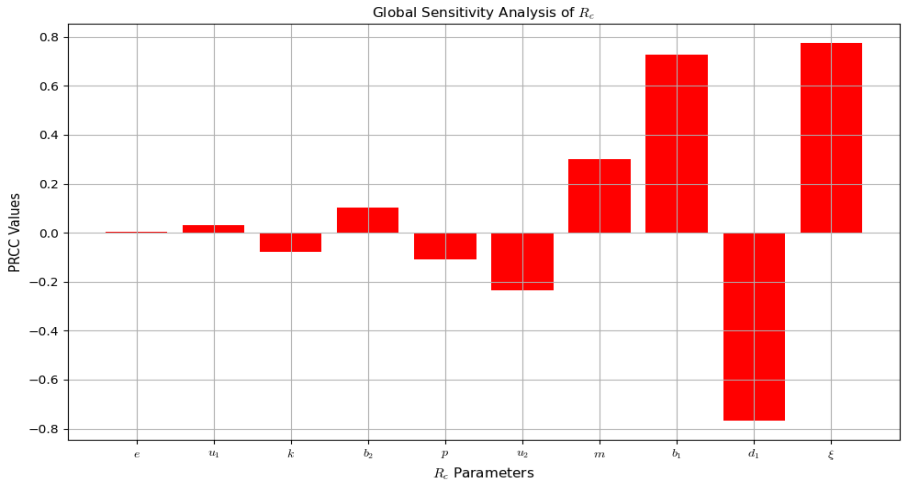


(a)

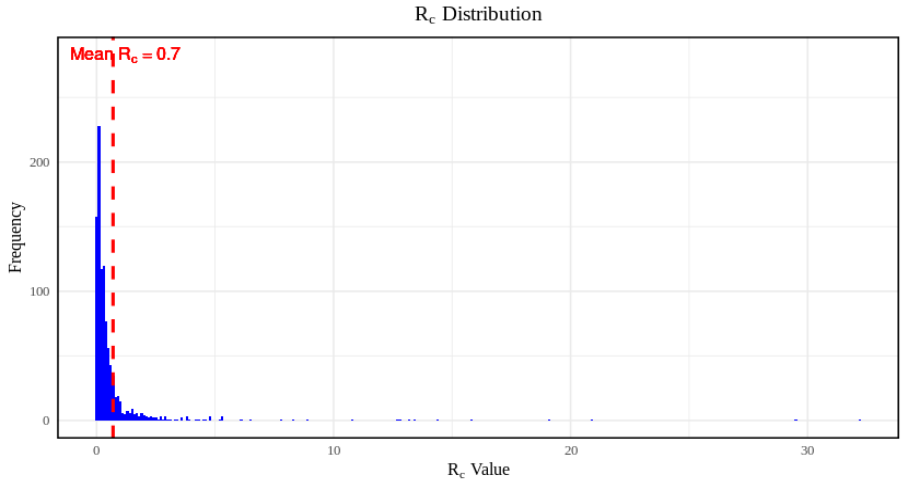


(b)

**Figure 3.** (a) Global sensitivity analysis using LHS (b) Distribution for the reproduction number $\mathcal{R}_c$ during 1000 runs during the global sensitivity analysis using LHS.

Based on the data presented in Table 3 and Figure 3(a), it is clear that $b_1$ and $\xi$ exhibit the highest positive PRCC values coupled with the lowest p-values, indicating their strong influence on the model. These results highlight the importance of controlling the TB infection rate, whether through pharmaceutical means such as vaccination or by utilizing self-defense mechanisms against infection, such as wearing proper face masks. In contrast, $d_1$ demonstrates a significantly negative PRCC value with a low p-value less than 0.05, highlighting its substantial impact. Thus, controlling the spread of

TB infectious diseases can be achieved by reducing $b_1$ and $\xi$ while increasing the rate of $d_1$. For more on the global sensitivity analysis, interested readers can also reference the following mathematical modeling framework [1, 39–44] that has applied this approach. Furthermore, our results in Figure 3 in panel (b) show the distribution of $\mathcal{R}_c$ using 1000 samples of parameter sets. In this simulation, we observe that the mean of $\mathcal{R}_c$ in Indonesia, according to our model, is below one, indicating that TB could potentially be eliminated from Indonesia if the current public health policies on TB are maintained or further enhanced.

### 5.2.2. Two-parameter sensitivity analysis

We present a two-parameter sensitivity analysis of $\mathcal{R}_c$ with respect to the proportion of face mask usage ($u_1$) and the rate of media campaigns ($u_2$) in Figure 4(a) and between proportion of slow progression ($p$) with proportion of success treatment ($k$) in Figure 4(b). From Figure 4(a), increasing the proportion of people using face masks and intensifying media campaigns reduces the reproduction number. A smaller reproduction number increases the likelihood of TB elimination. The more intense the media campaign, the smaller the proportion of people who need to use face masks to achieve $\mathcal{R}_c < 1$. Combining both interventions will alleviate the burden on the government in eradicating TB from the population. Figure 4(b) shows the level set of $\mathcal{R}_c$ with respect to $p$ and $k$. It is seen that a higher probability of slow progression reduces $\mathcal{R}_c$. Biologically, this means that more infected individuals do not immediately progress to active TB, which delays the transmission to others. Similarly, a higher probability of successful treatment also reduces $\mathcal{R}_c$. To increase the probability of successful treatment, several interventions can be implemented, such as enhancing monitored treatment efforts or improving the quality of TB medicine.

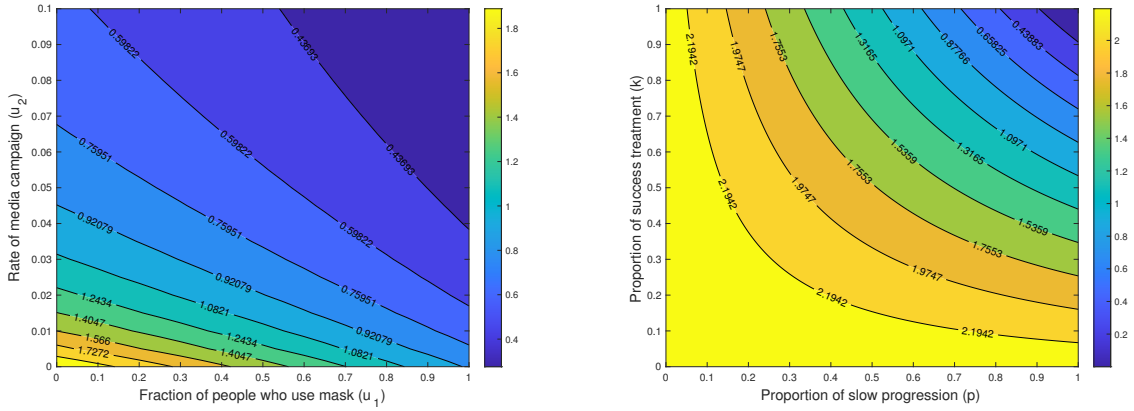


(a) (b)

**Figure 4.** Contour plot of $\mathcal{R}_c$ with respect to face mask use ($u_1$) and media campaign ($u_2$) in panel (a), and between proportion of slow progression ($p$) with proportion of success treatment ($k$) in panel (b). All parameters are provided in Section 5.1.

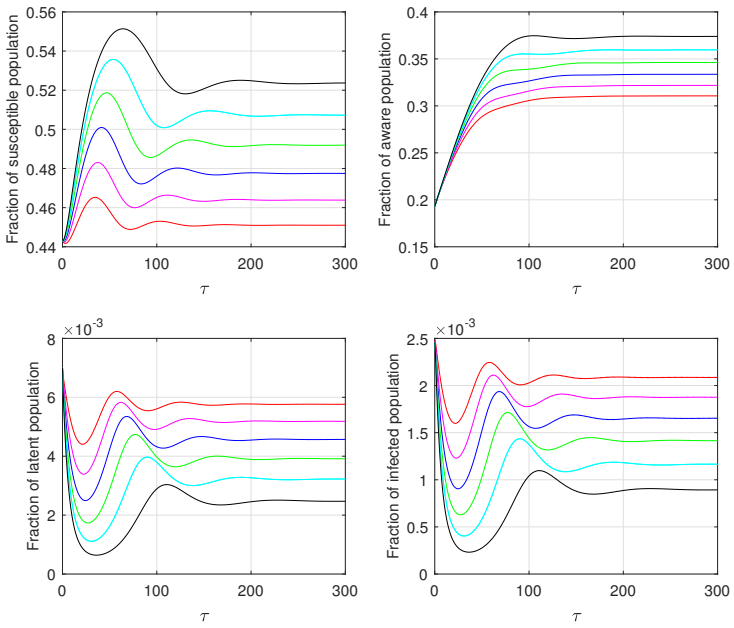


**Figure 5.** Numerical simulation of $x_1$, $x_2$ (first row) and $x_3$, $x_4$ (second row), from left to right, respectively, showing the impact of medical mask use $u_1$. All parameters are provided in Section 5.1, except $u_1$ which varies.

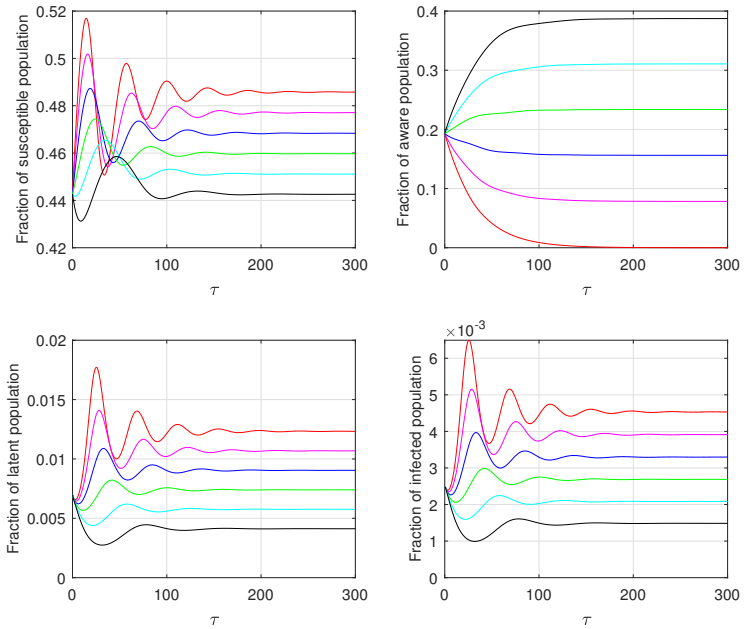


**Figure 6.** Numerical simulation of $x_1$, $x_2$ (first row) and $x_3$, $x_4$ (second row), from left to right, respectively, showing the impact of media campaign ($u_2$). All parameters are provided in Section 5.1, except $u_2$, which varies.

To show the impact of mask usage and media campaign interventions on the dynamics of each compartment $x_1, x_2, x_3$, and $x_4$, we conduct an autonomous simulation, as shown in Figures 5 and 6. Figure 5 presents the results for varying values of $u_1$ from $0, 0.1, 0.2, 0.3, 0.4$, and $0.5$. The smallest $u_1$ value is represented by the red curve, while the largest $u_1$ value is represented by the black curve. It is evident that increasing mask usage successfully increases the number of susceptible individuals ($x_1$ and $x_2$) while reducing the number of infected individuals ($x_3$ and $x_4$). Figure 6 displays the changes in the variables $x_1, x_2, x_3$, and $x_4$ as $u_2$ increases from 0 (shown by the red curve) to 0.0125 (represented by the black curve). In a similar manner, intensifying the media effort can enhance the number of susceptible individuals while decreasing the number of infected individuals.

### *5.3. Bifurcation diagram and autonomous simulation*

From Theorems 2 and 4–7, we demonstrate that system (2.3) always has a stable disease-free equilibrium point $\mathcal{E}_0$ if $\mathcal{R}_c < 1$. Conversely, it always has a stable endemic equilibrium point $\mathcal{E}_1$ if $\mathcal{R}_c > 1$. Additionally, bistability between $\mathcal{E}_0$ and $\mathcal{E}_1$ is possible for $\mathcal{R}_c^* < \mathcal{R}_c < 1$ if $c < c^*$. Parameter $c$ plays a critical role in regulating the saturation of hospital treatment capacity. A larger value of $c$ implies a greater intrinsic treatment capacity, so the recovery rate is less affected by rising hospitalization. Smaller $c$ can contribute to the occurrence of backward bifurcation and the persistence of the disease even when $\mathcal{R}_0 < 1$. In contrast, a larger $c$ reflects higher hospital capacity, which not only improves patient outcomes but also reduces the likelihood of complex bifurcation behavior, thereby simplifying disease control strategies.

Furthermore, the possible occurrence of periodic solutions through Hopf bifurcation phenomena also has been analyzed. In this section, we present numerical experiments to confirm these phenomena. We use all parameter values estimated in the previous section, except for $b_1$, which serves as the bifurcation parameter, and $c$, which serves as $\mathscr{A}$. From Theorem 7, it has been shown that forward bifurcation occurs at $\mathcal{R}_c = 1$ if $\mathscr{A} < 0$. On the other hand, backward bifurcation appears when $\mathscr{A} > 0$.

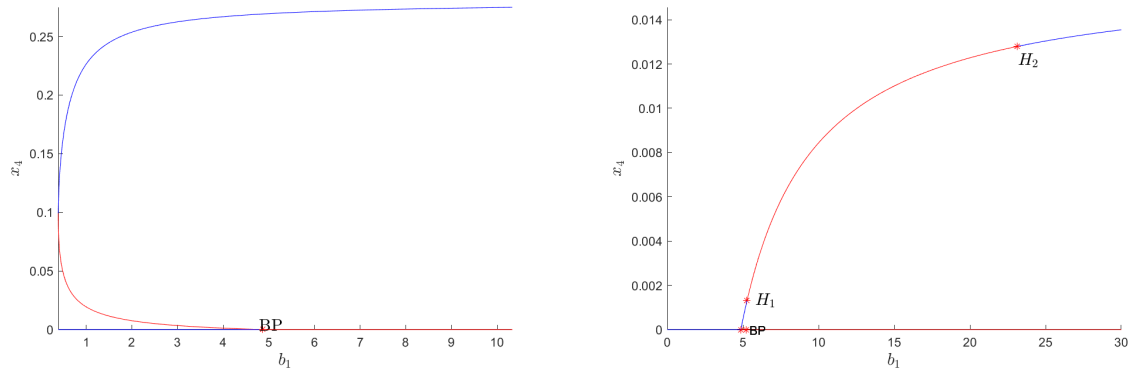


(a) (b)

**Figure 7.** Bifurcation diagram of system (2.3) at $\mathcal{R}_0 = 1$ shows a backward bifurcation phenomena when $c = 3.73 \times 10^{-7} < c^*$ in panel (a), and a forward bifurcation phenomena when $c = 1.86 \times 10^{-6} > c^*$ in panel (b).

Using the best-fit parameter from the previous section, we find that $c^* = 9.349 \times 10^{-7}$. The first

numerical experiments are given in Figure 7, where we choose $c = 0.4c^*$ to give a backward bifurcation phenomena, as shown in Figure 7(a), and $c = 2c^*$ to give a forward bifurcation phenomena, as shown in Figure 7(b). From Figure 7(a), for $b_1 = 0$ and increasing, we have a stable disease-free equilibrium point $\mathcal{E}_0$ until it reaches its branching point ($BP$), or where $b_1 = 4.86$ such that $\mathcal{R}_c = 1$. At $BP$, $\mathcal{E}_0$ changes it stability from stable to unstable and remains unstable for all $b_1 > BP$. Moving to the other branch, since $c < c^*$, we have an unstable endemic equilibrium point from $b_1 < BP$ until it reaches the Fold Point, which is denoted by the interchange between red and blue curves on the branch. There is a multiple endemic equilibrium that appears for some value of $\mathcal{R}_c < 1$, where the smaller endemic equilibrium point is unstable, while the larger one is stable. This enables the possibility of a bistability phenomenon when $\mathcal{R}_c < 1$. For $b_1 = 2$, the solution may converge to either a stable disease-free equilibrium point or a stable endemic equilibrium point (Figure 8). Conversely, when bistability does not occur, the solution consistently converges to the same stable equilibrium point. As illustrated in Figure 9, selecting $b_1 = 0.1$ causes the solution to converge to a stable disease-free equilibrium point.

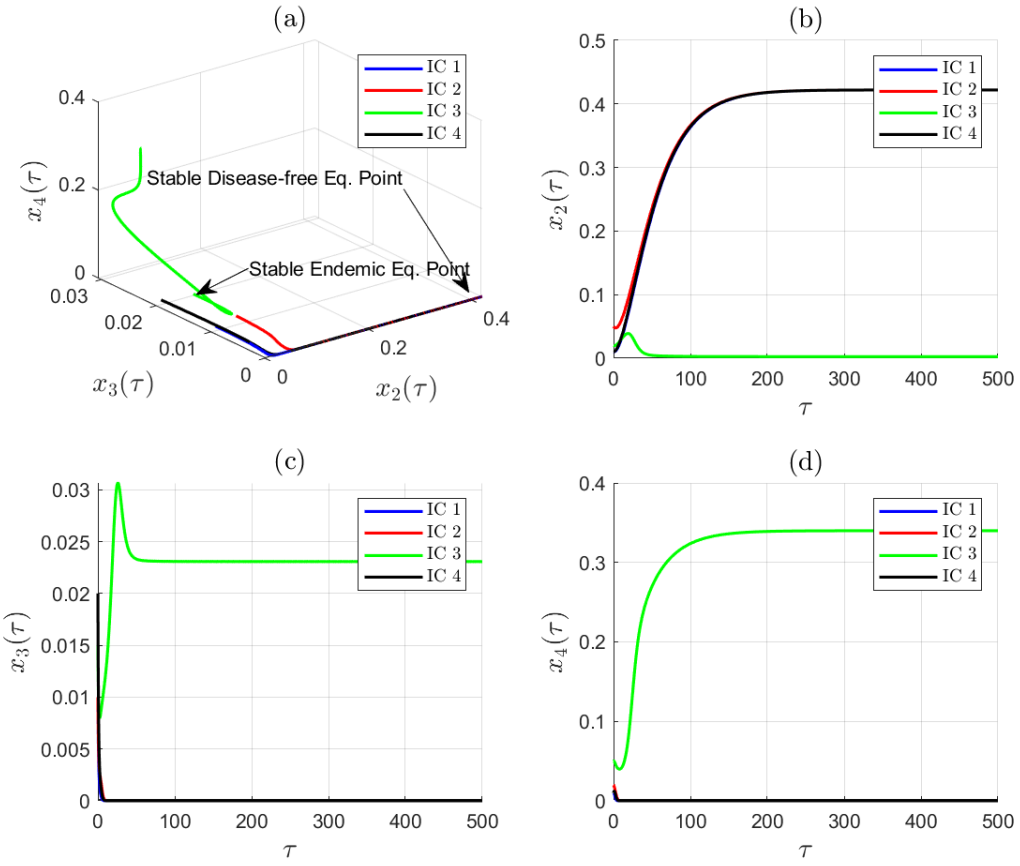


**Figure 8.** Time series demonstrating bistability corresponding to selected points on the bifurcation diagram in Figure 10(a), with parameter values $b_1 = 2$ and four different initial conditions, confirming the coexistence of multiple attractors. Each panel shows the trajectories in (a) $x_2 - x_3 - x_4$, (b) $\tau - x_2$, (c)$\tau - x_3$, and (d) $\tau - x_4$ plane.

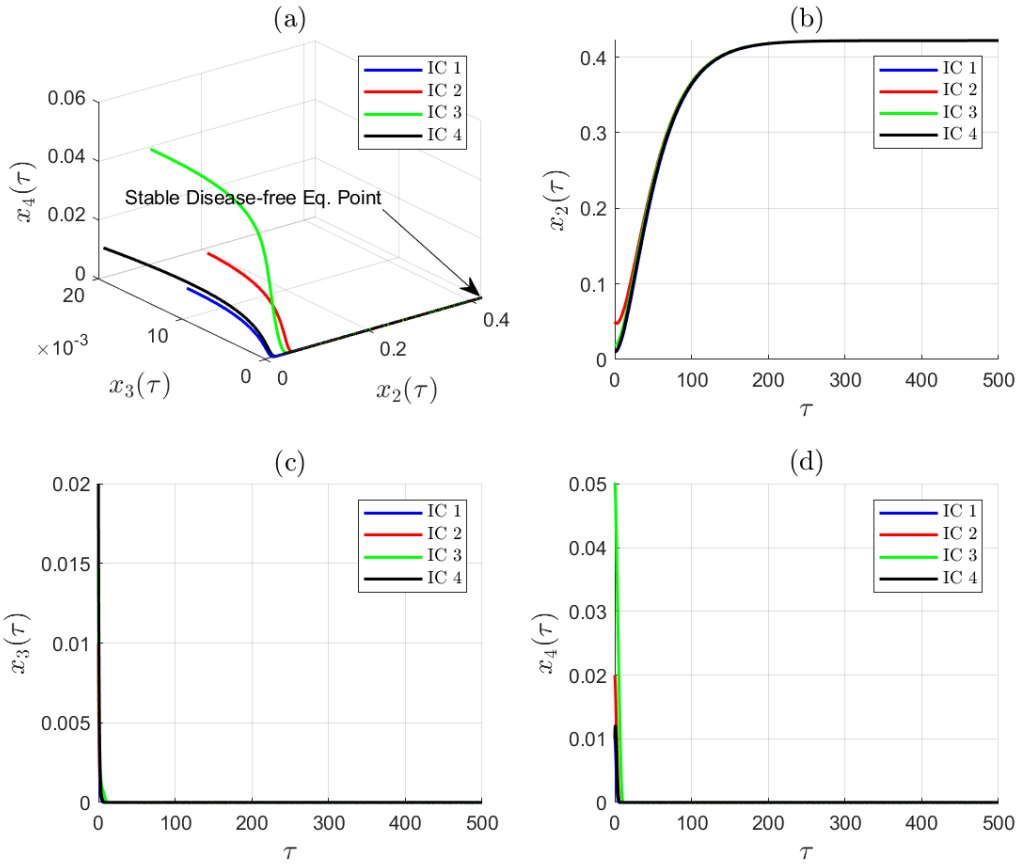


**Figure 9.** The sample of solution tends to the asymptotic stable disease-free equilibrium point corresponding to selected points on the bifurcation diagram in Figure 10(a), with parameter values $b_1 = 0.1$ and four different initial conditions. Each panel shows the trajectories in (a) $x_2 - x_3 - x_4$, (b) $\tau - x_2$, (c)$\tau - x_3$, and (d) $\tau - x_4$ plane.

In the case of a forward bifurcation phenomenon illustrated in Figure 7(b), the disease-free equilibrium point is locally stable for $b_1 < BP$. Upon reaching the branching point $BP$ at $b_1 = 4.86$, the disease-free equilibrium point loses its stability and remains unstable for all $b_1 \geq BP$. Furthermore, a unique stable endemic equilibrium point begins to appear as $b_1$ increases, until it reaches the first Hopf point $H_1$ at $b_1 = 5.266$. At this point, the stability of the endemic equilibrium point changes to a stable periodic solution until it reaches the second Hopf point $H_2$ at $b_1 = 23.12$. The family of the stable limit cycle between the two Hopf points are given in Figure 10(a) with the period for each limit cycle is given in Figure 10(b). It can be seen that the smaller $b_1$ when $b_1 \in [H_1, H_2]$ then the period becomes larger. Beyond Hopf point $H_2$, the endemic equilibrium point becomes asymptotically stable again. The autonomous simulation for $b_1 = 15$ is shown in Figure 11. Since $b_1 = 15$ lies between $H_1$ and $H_2$, the solution tends toward a stable limit cycle, as demonstrated in Figure 11(a). As shown in panels (b)–(d) of Figure 11, we can see that all solutions converge to the stable limit cycle. Conversely, when $b_1$ exceeds $H_2$, the endemic equilibrium point becomes asymptotically stable again, as shown in Figure 12.

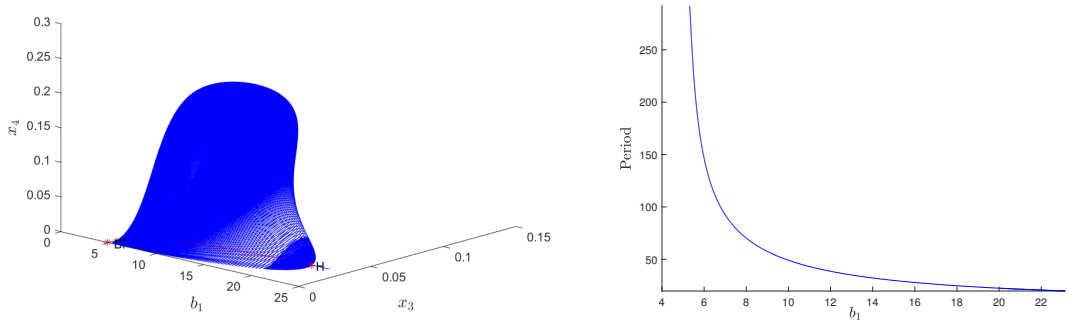


(a) (b)

**Figure 10.** (a) Families of periodic solutions for $c = 1.86 \times 10^{-6}$ and (b) corresponding period of the periodic solutions over the range $b_1 \in [H_1, H_2]$.

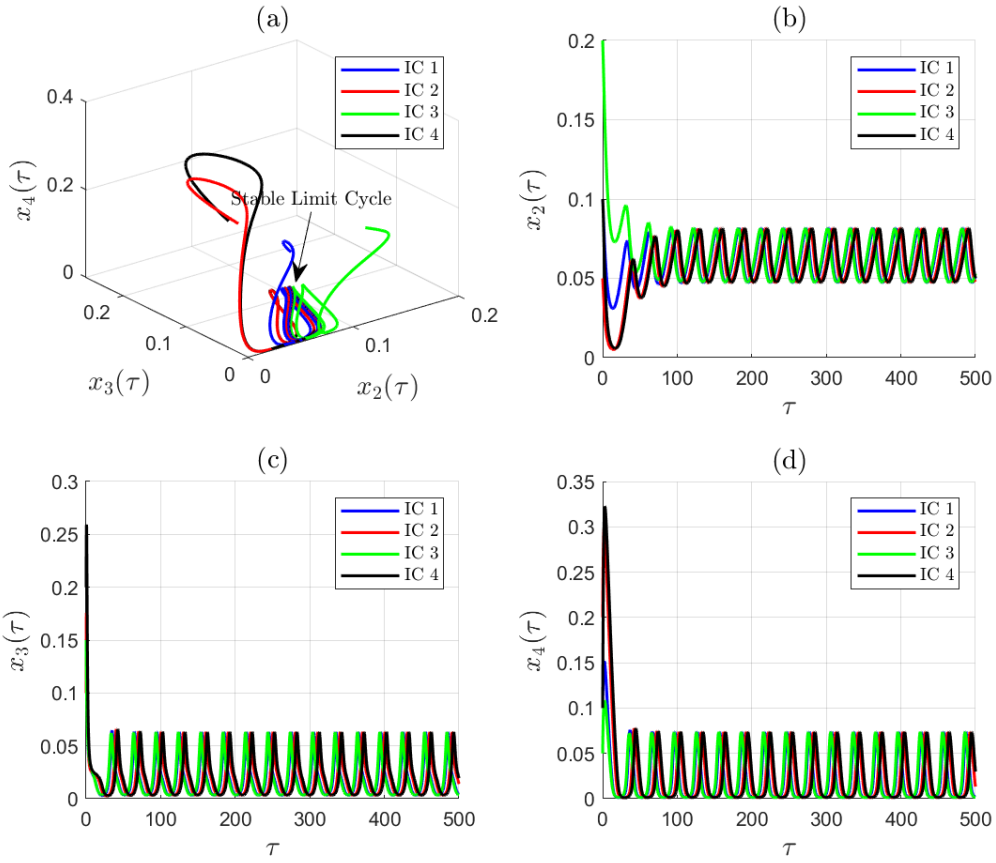


**Figure 11.** The sample of periodic solution corresponding to selected points on the bifurcation diagram in Figure 10(b), with parameter values $b_1 = 15$ and four different initial conditions. Each panel shows the trajectories in (a) $x_2$–$x_3$–$x_4$, (b) $\tau$–$x_2$, (c)$\tau$–$x_3$, and (d) $\tau$–$x_4$ plane. These plots illustrate the dynamic behavior of the system on the periodic branches.

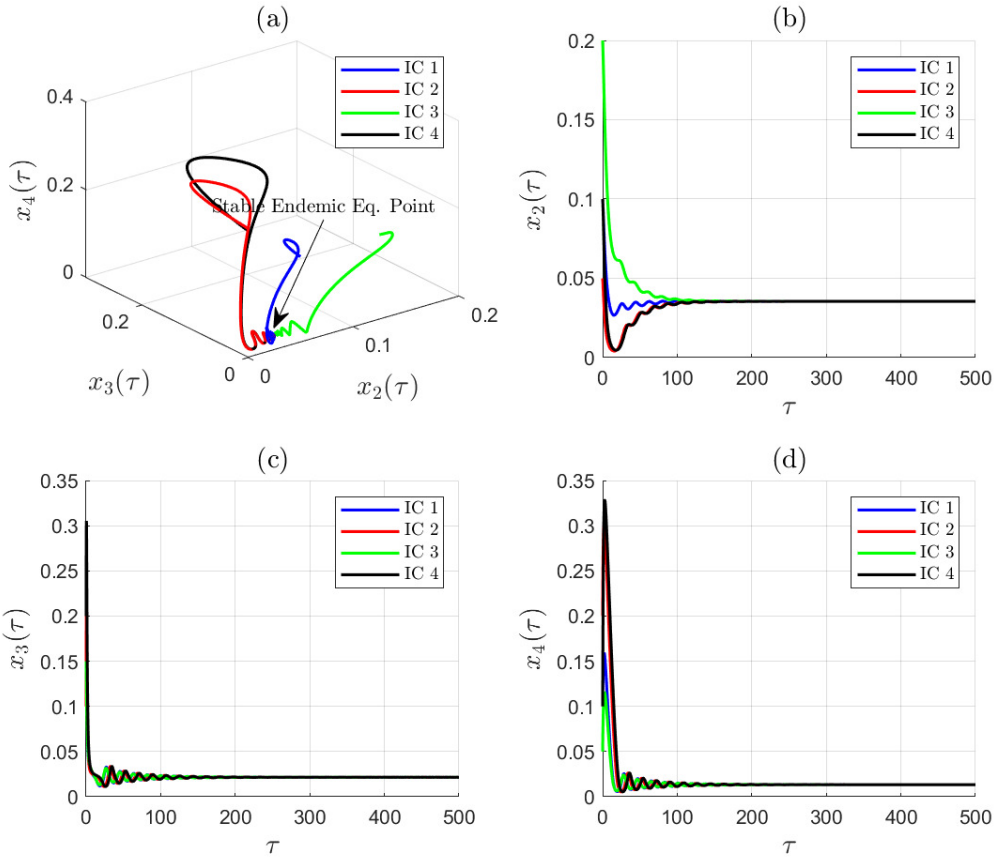


**Figure 12.** The sample of solution tends to an asymptotic stable endemic equilibrium point corresponding to a selected points on the bifurcation diagram in Figure 10(b), with parameter values $b_1 = 27$ and four different initial conditions. Each panel shows the trajectories in (a) $x_2 - x_3 - x_4$, (b) $\tau - x_2$, (c)$\tau - x_3$, and (d) $\tau - x_4$ plane. These plots illustrate the dynamic behavior of the system on the stable endemic equilibrium point branches.

## 6. Optimal control model

### *6.1. Optimal control modeling*

From our previous analysis, we can see that increasing the proportion of individuals who use masks or increasing the intensity of media campaigns can significantly reduce the reproduction number, which in the end may eliminate TB. However, because of the intensity of this intervention, the cost will be higher. Hence, an optimal intervention needs to be justified, which is an intervention that depends on the needs. Hence, the intervention should depend on the epidemic status and time. The control parameters should be time-dependent variables. Based on this assumption, we define our control parameter in Eq (2.3) as a new time-dependent control variable, namely $u_1(t)$ and $\bar{u_2}(t)$, which represent the mask use and media campaign intervention.

Based on the above assumptions, our non-dimensional TB model in (2.3) now read as follows:

$$\begin{aligned}
\frac{dx_1}{d\tau} &= m(1-x_1) + ex_2 - (1-u_1(t)\xi)b_1x_1x_4 - u_2(t)x_1,\\
\frac{dx_2}{d\tau} &= u_2(t)x_1 - (1-u_1(t)\xi)b_2x_2x_4 - (e+m)x_2,\\
\frac{dx_3}{d\tau} &= (1-u_1(t)\xi)pb_1x_1x_4 + (1-u_1\xi)b_2x_2x_4 - (1+m)x_3,\\
\frac{dx_4}{d\tau} &= (1-u_1(t)\xi)(1-p)b_1x_1x_4 + (1-k)x_3 - \left(d_1 - \frac{d_2x_4}{c+bx_4}\right)x_4 - mx_4.
\end{aligned} \tag{6.1}$$

Our goal is to reduce the number of infected people $x_3(t)$ and $x_4(t)$ while using the least amount of force for our interventions, $u_1(t)$ and $u_2(t)$. The following cost function reflects these objectives:

$$\mathcal{J}(u_1(t), u_2(t), x_3(t), x_4(t)) = \int_0^{t_f} \left(\omega_1 x_3(t) + \omega_2 x_4(t) + \varphi_1 u_1^2 + \varphi_2 u_2^2\right) dt, \tag{6.2}$$

where $\omega_1$ and $\omega_2$ are positive weight parameters for $x_3(t)$ and $x_4(t)$, respectively, while $\varphi_1$ and $\varphi_2$ present positive weight parameters for $u_1(t)$ and $u_2(t)$, respectively. The purpose of these weight settings is to balance each component on $\mathcal{J}$ so that no component gains greater dominance than any other. Thus, $\frac{\omega}{\varphi} \approx \frac{u(t)}{x(t)}$ must be satisfied. We write $x_i(t)$ for $i = 1, 2, 3, 4$ as $x_1$ and $u_1(t)$ for $i = 1, 2$ as $u_i$ to simplify things.

### *6.2. Optimal control characterization*

We characterize the optimal control $u^* = (u_1^*, u_2^*)$ which will gives an optimal value of $\mathcal{J}$ and optimal solution of $x_1^*, x_2^*, x_3^*$, and $x_4^*$. The necessary condition for the optimal controls are obtained from using the Pontryagin's Maximum Principle (PMP). First, we define the Hamiltonian function as follows:

$$\begin{aligned}
\mathcal{H} &= \omega_1 x_3(t) + \omega_2 x_4(t) + \varphi_1 u_1^2 + \varphi_2 u_2^2 \ldots\\
&+ \lambda_1 \left(m(1-x_1) + ex_2 - (1-u_1(t)\xi)b_1x_1x_4 - u_2(t)x_1\right) \ldots\\
&+ \lambda_2 \left(u_2(t)x_1 - (1-u_1(t)\xi)b_2x_2x_4 - (e+m)x_2\right) \ldots\\
&+ \lambda_3 \left((1-u_1(t)\xi)pb_1x_1x_4 + (1-u_1\xi)b_2x_2x_4 - (1+m)x_3\right) \ldots\\
&+ \lambda_4 \left((1-u_1(t)\xi)(1-p)b_1x_1x_4 + (1-k)x_3 - \left(d_1 - \frac{d_2x_4}{c+bx_4}\right)x_4 - mx_4\right),
\end{aligned} \tag{6.3}$$

where $\lambda_i$ for $i = 1, 2, 3, 4$ are the adjoint variables.

**Theorem 8.** *Let $X = (x_1, x_2, x_3, x_4)$ and $u = (u_1, u_2)$. Let $u^*$ be the optimal control pair, then there exists an adjoint variable $\lambda_i(t)$ for $i = 1, 2, 3, 4$, satisfying the following system of ordinary*

*differential equations:*

$$\begin{aligned}
\frac{d\lambda_1}{dt} &= (1-u_1\xi)(1-p)b_1x_4(\lambda_1-\lambda_4)+(1-u_1\xi)pb_1x_4(\lambda_1-\lambda_3)+u_2(\lambda_1-\lambda_2)+m\lambda_1,\\
\frac{d\lambda_2}{dt} &= (1-u_1\xi)b_2x_4(\lambda_2-\lambda_3)+e(\lambda_2-\lambda_1)+m\lambda_2,\\
\frac{d\lambda_3}{dt} &= -\omega_1+(\lambda_3-\lambda_4)+k\lambda_4+m\lambda_3,\\
\frac{d\lambda_4}{dt} &= -\omega_2+p(1-u_1\xi)b_1x_1(\lambda_1-\lambda_3)+(1-p)(1-u_1\xi)b_1x_1(\lambda_1-\lambda_4)\ldots\\
&\quad+(1-u_1\xi)b_2x_2(\lambda_2-\lambda_3)+\lambda_4\left(d_1-\frac{d_2x_4(2/N+bx_4)}{(1/N+bx_4)^2}\right)+m\lambda_4,
\end{aligned} \tag{6.4}$$

*with a transversality condition*

$$\lambda_i(t_f)=0, i=1,2,3,4,$$

*and optimal controls:*

$$\begin{aligned}
u_1^* &= \min\left\{1,\max\left\{0,\frac{\xi x_4}{2\varphi_1}\left(b_2x_2(\lambda_3-\lambda_4)+b_1x_1[(\lambda_4-\lambda_1)-p(\lambda_4-\lambda_3)]\right)\right\}\right\},\\
u_2^* &= \min\left\{1,\max\left\{0,\frac{x_1}{2\varphi_2}(\lambda_1-\lambda_2)\right\}\right\}.
\end{aligned} \tag{6.5}$$

*Proof.* With the Hamiltonian function given in Eq (6.3), the proof of the theorem is a direct consequence of Pontryagin's Maximum Principle. The adjoint system and its transversality conditions are taken from:

$$\frac{d\lambda_i}{dt}=-\frac{\partial\mathcal{H}}{\partial x_i}, \quad \text{for } i=1,2,3,4.$$

Since all the state variables $x_i$ are free at $t_f$, then the transversality conditions is given by

$$\lambda_i(t_f)=0, i=1,2,3,4.$$

The optimal control $u_i^*$ is taken from the solution $\dfrac{\partial\mathcal{H}}{\partial u_i}=0$ with respect to $u_i$ for $i=1,2$, and including the standard argument that the control variables should be between 0 and 1.

### *6.3. Numerical experiments on the optimal control problem*

To conduct our numerical experiment on the optimal control problem, we use the same set of parameter values as given in Section 5.1, except we set $b_1=6.4, \omega_1=1, \omega_2=1, \varphi_1=0.1$, and $\varphi_2=5$. To solve the optimal control problem, we use a forward-backward sweep method [45]. This method is well known to be used to solve an optimal control problem numerically, including in mathematical epidemiology models [46–49]. The algorithm is as follows:

Step 1. We solve the state system in Eq (6.1) forward in time by setting $u_i=0$ as a base when control is not implemented. We also calculate the cost function $\mathcal{J}$.

Step 2. To solve the optimal control problem, we start by setting an initial guess for $u_1$ and $u_2$ for $t\in[0,t_f]$. Here, we use a constant initial guess.

Step 3. Solve the state system in system (6.1) forward in time using the initial guess of $u_i$ and the initial condition of $x_i$ for $i = 1, 2, 3, 4$.

Step 4. Using the results from Step 3, solve the adjoint system in (6.4) backward in time using the transversality condition $\lambda_i(t_f) = 0$. for $i = 1, 2, 3, 4$.

Step 5. Update the control $u_i(t)$ for $i = 1, 2$ using the formula in (6.5), and update the cost function $\mathcal{J}$.

Step 6. Continue with Step 3 using an updated $u_i(t)$ until the convergence criteria are achieved. In our case, we terminate the iteration whether the difference of $\mathcal{J}$ from iteration $k$ and $k + 1$ is less than $10^{-3}$ or the iteration reaches 100 times.

In the following subsection, we conduct our numerical experiments based on several scenarios, including different combinations of strategies, varying unit costs of interventions, and the impact of slow-fast progression.

### 6.3.1. Different combinations of interventions

The first numerical experiment conducted for the optimal control problem focuses on the combination of interventions we aim to implement. Consequently, we have three scenarios for control implementation. The first scenario involves using face masks as the sole intervention to minimize the spread of TB. In this scenario, we set $u_2(t) = 0$ for all $t \in [0, t_f]$, while $u_1(t)$ is allowed to vary between 0 and 1. The results are presented in Figure 13. It can be observed that implementing face masks as a single intervention only slightly reduces the number of infected individuals and delays the peak of the outbreak for a short period. The dynamics of $u_1$ are shown in panel (e) of Figure 13, while the dynamics of $x_1$ to $x_4$ are illustrated in panels (a) to (d).

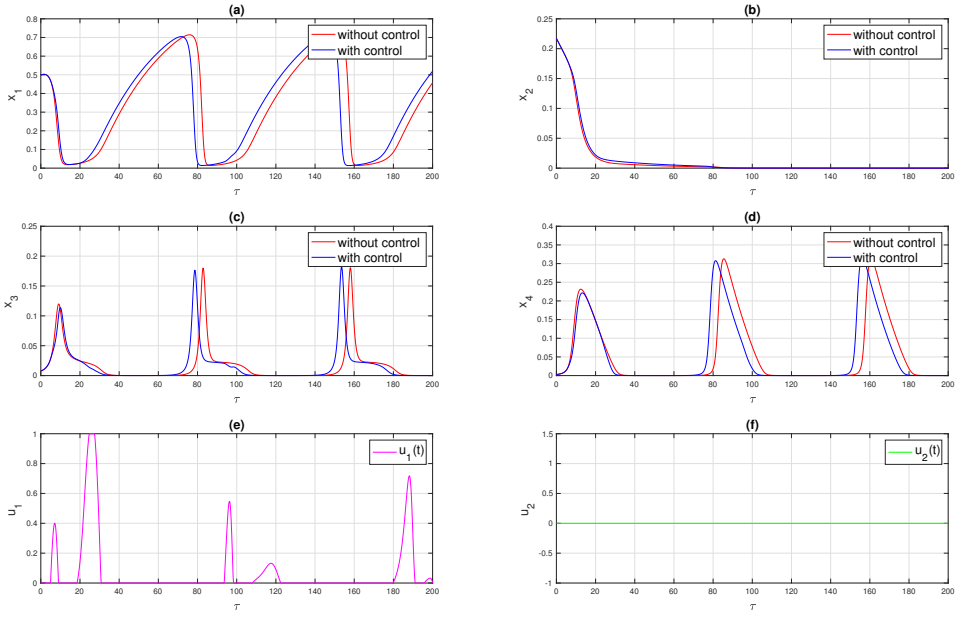


**Figure 13.** Optimal control simulation when face masks are implemented as a single intervention.

The next scenario is when we use media campaigns as a single intervention to prevent the massive spread of TB. Hence, we set $u_1 = 0$ for all $t \in [0, t_f]$. The results are given in Figure 14. Compared with the previous scenario where we use only face masks as a single intervention, the results of using media campaigns as a single intervention are not trivial in combating the spread of TB. It can be seen that the number of people becoming aware of TB increases significantly (see panel (b) in Figure 14). As a result, the frequency of outbreaks during the simulation period can be reduced. Without any control measures, there are three outbreaks. On the contrary, implementing a media campaign successfully reduces the number of outbreaks to just one during the same simulation interval, as shown in panels (c) and (d). However, the severity of the outbreak with control implementation is slightly higher compared to the case with no control. The dynamics of healthy individuals who are not aware can be seen in panel (a), while the infected individuals are shown in panels (c) and (d). The dynamics of the media campaign control are displayed in panel (f), where the intervention is intense at the beginning and end of the simulation but low in the middle.

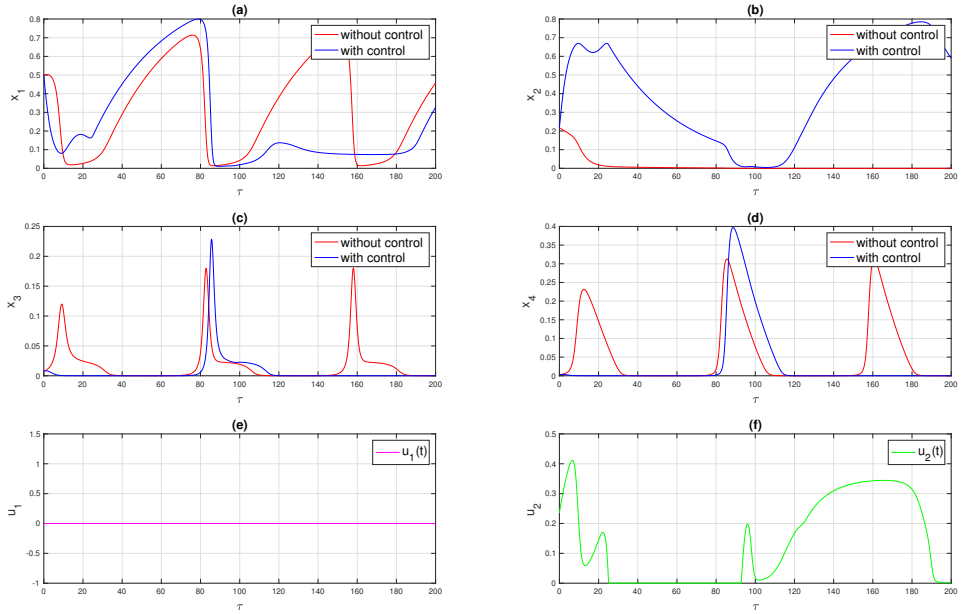


**Figure 14.** Optimal control simulation when media campaigns are implemented as a single intervention.

The final scenario involves the simultaneous implementation of face masks and media campaigns. The results are depicted in Figure 15. Compared to the first and second scenarios, combining face masks and media campaigns is more effective in reducing the spread of TB. The intensity of the media campaign is lower compared to the second scenario, as in this scenario, the face mask intervention serves as a complementary measure. The dynamics of the controls are shown in Figure 15, panels (e) and (f). As a result, the number of susceptible individuals who are aware increases significantly, as shown in panels (a) and (b). Panels (c) and (d) illustrate the dynamics of infected individuals. Compared to the second scenario, the number of the reduced outbreak is the same. However, the level of outbreak is smaller and and it occurs more quickly than in scenario 2.

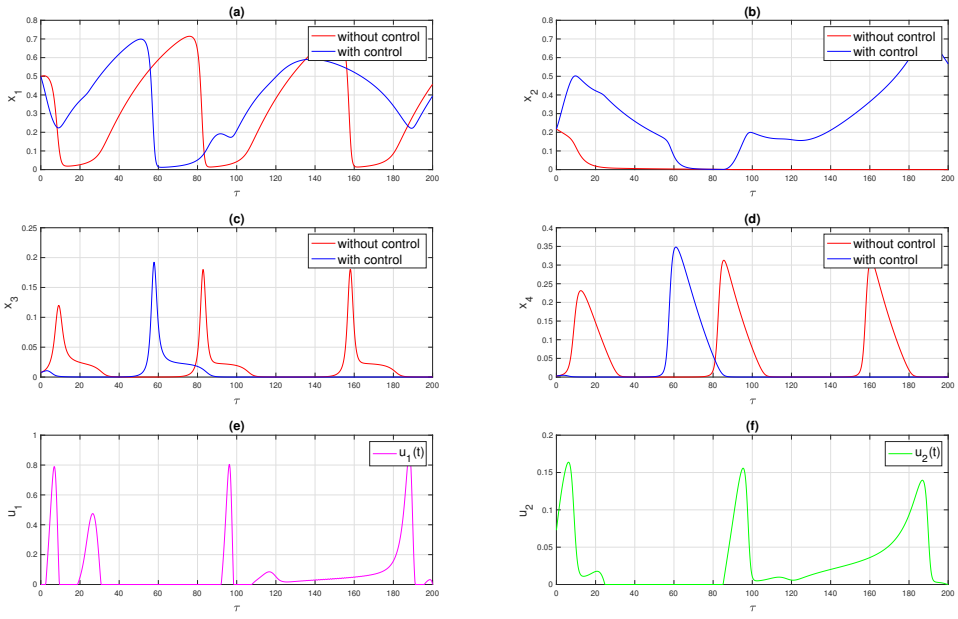


**Figure 15.** Optimal control simulation when face masks and media campaigns are implemented together.

From these three simulations, we can conclude that while face masks and media campaigns have the potential to prevent the rapid spread of TB, the simultaneous implementation of both strategies should be considered the best intervention. This is because the two strategies target different aspects of prevention. Media campaigns focus on increasing public awareness of TB, encouraging people to be more cautious about direct contact with infected individuals, while the use of face masks provides a practical means for individuals to protect themselves from direct contact. Therefore, both strategies should be implemented together to achieve better results.

### 6.3.2. Impact of a cheaper unit cost for controls

In the previous section, we observed that implementing face masks and media campaigns simultaneously is the most effective strategy for reducing the spread of TB. In this section, we conduct a simulation using both interventions but with a reduced unit cost for control (smaller $\varphi_1$ and $\varphi_2$) and compare it with the results in Figure 15. Specifically, we reduce $\varphi_1$ and $\varphi_2$ to just one-fifth of their previous values. The results are presented in Figure 16. It can be observed that with the lower unit cost for face masks and media campaigns, a more extensive intervention is achievable, as shown in panels (e) and (f) in Figure 16. Consequently, the number of infected individuals decreases significantly to zero (see panels (c) and (d)), while the number of susceptible individuals, both aware and unaware, increases significantly (see panels (a) and (b)). According to our prior simulation, we have determined that decreasing the cost of interventions, such as face masks and media campaigns, can result in a broader and more successful implementation of these methods. Consequently, the transmission of TB can be more efficiently managed, potentially leading to a complete elimination of infected persons. This implies that the cost-effectiveness of public health initiatives is essential since

it enables a wider and more influential implementation, therefore improving the overall effectiveness of disease control efforts.

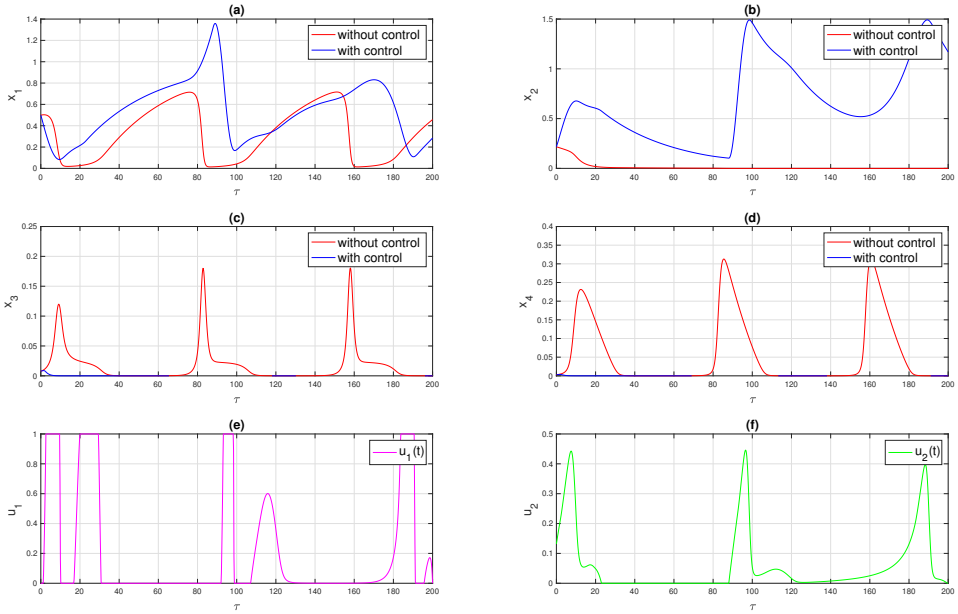


**Figure 16.** Optimal control simulation when face masks and media campaigns are implemented together, but with a smaller unit cost where $\varphi_1 = 0.02$ and $\varphi_2 = 1$.

### 6.3.3. Impact of bigger probability of fast TB progression (smaller $p$)

From Table 3 and Figure 4(b), we found that the proportion of slow TB progression plays a crucial role in determining the reproduction number. A smaller $p$ gives a bigger reproduction number and indicates that more individuals experience fast progression of TB to active TB status. Biologically, this suggests that a higher proportion of individuals experiencing fast progression is worsening the TB endemic situation. Therefore, it is important to analyze the impact of TB control when $p$ is smaller.

To conduct the simulation, we set the parameter value of $p$ to 50% of its original value and compared the results with those from Figure 15. The results depicted in Figure 17, panels (e) and (f), show that when more people experience fast progression, a more intensive intervention is required compared to when $p$ is larger. Specifically, with a smaller $p$, a high intensity of face mask use and media campaigns should be followed by a moderate level of intervention shortly after the peak intervention. Furthermore, with a smaller $p$, the intensity of face mask use reaches 100% implementation three times, coinciding with TB outbreaks. Similarly, the intensity of media campaigns is also greater when $p$ is smaller.

Comparing the scenarios with larger and smaller $p$ in Figures 15 and 17, respectively, we observe that outbreaks occur three times when interventions are not implemented. A smaller $p$ results in a lower level of outbreak for $x_3$ (see the red curve in panel (c) in Figure 17) but a higher level of outbreak for $x_4$ (see the red curve in panel (d) in Figure 17). Despite the implementation of face masks and media campaigns in the case of a smaller $p$, the outcomes are not better compared to a larger $p$ scenario. In the case of a smaller $p$ in Figure 17, even with the controls in place, TB outbreaks still occur three

times within the simulation period. This is in stark contrast to the scenario with a larger $p$ in Figure 15, where the outbreak occurs only once in the same time interval.

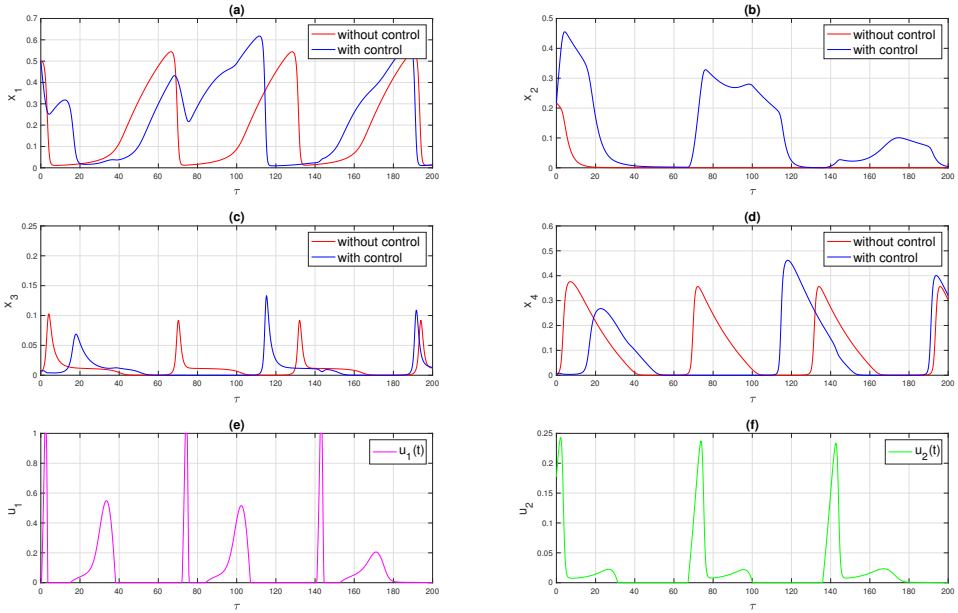


**Figure 17.** Optimal control simulation when face masks and media campaigns are implemented together, but with a bigger fast progression probability (smaller $p$).

From the optimal control simulation in this section, we conclude that when the fraction of individuals who experience fast progression to active TB (represented by smaller $p$), more intense and ongoing interventions, such as the use of face masks and media campaigns, are necessary to control the spread of TB. Nevertheless, despite the increased efforts, the results are less effective when compared to situations where a larger proportion of individuals experience slow progression (bigger $p$). More precisely, when the value of $p$ is smaller, there is a higher frequency of TB outbreaks. This suggests that the rapid advancement of the disease greatly hinders the efficiency of control methods. This emphasizes the crucial significance of focusing on the factors that impact the pace of progression in tuberculosis control programs.

## 7. Discussion and conclusions

In this paper, we investigate a novel $SALIR$ TB model that incorporates the impact of media campaigns, face masks, slow-fast progression, and a saturated recovery rate. We rigorously analyze the model concerning the existence and stability of equilibrium points and how the reproduction number determines the stability and existence criteria. Interestingly, our model may exhibit a backward bifurcation phenomenon when the reproduction number equals one, particularly if the effect of hospital bed capacity increases. This implies the co-existence of TB-free and TB-endemic equilibrium points even when the reproduction number is less than one. This presents a significant challenge for TB control strategies, as reducing the reproduction number to less than one no longer

guarantees the eradication of TB from the population.

Our model parameters were estimated using incidence data from Indonesia, which can be accessed from [37]. Based on this set of parameters, we conducted a global sensitivity analysis and found that media campaigns are more promising in reducing TB compared to the use of face masks. From the forward bifurcation diagram, we discovered a family of periodic solutions when the reproduction number is greater than one. A periodic solution suggests that the number of TB cases can vary over time, resulting in repeated outbreaks even when interventions are implemented. This implies that the entire eradication of TB may not be achievable; instead, its prevalence may fluctuate in alternating episodes of growth and decline. The existence of periodic solutions suggests that a constant or one-time interventions may not be enough to effectively control TB. For instance, if face masks and media campaign efforts are solely employed during the initial outbreak, they may temporarily decrease the number of infections, but they will not prevent future resurgences. On the contrary, our model proposes that these interventions must be maintained or modified over time, especially during periods of increasing illness prevalence. Additionally, the periodic occurrence of the outbreaks may be influenced by the point at which treatment capacity reaches its maximum limit. This means that during periods of high demand, healthcare systems may become overburdened, leading to a decrease in the effectiveness of interventions. It is crucial to not only sustain but significantly expand interventions such as face masks and media campaigns during these periods.

An optimal control model was introduced in this article, treating face masks and media campaigns as time-dependent interventions. Pontryagin's Maximum Principle was used to characterize the optimal control problem, which was then solved numerically using the forward-backward sweep method. Numerical experiments on the optimal control problem demonstrate how time-dependent media campaigns and face mask interventions can successfully reduce the spread of TB when implemented together. Our simulations show that the more people experience fast TB progression, the more intense the face mask use and media campaigns must be to effectively control the spread of TB.

The mathematical findings described in our research have important implications for public health strategies aimed at managing TB. The identification of a backward bifurcation, where TB can persist even when the reproduction number falls below one, emphasizes the complexity of eradicating this illness. This observation challenges the conventional approach that focuses on reducing the reproduction number, suggesting that broader strategies are required. In addition, our sensitivity analysis indicates that media campaigns are a more efficacious method for halting the transmission of tuberculosis compared to the use of face masks. This highlights the importance of dedicating resources to public awareness and education as essential components of tuberculosis control efforts. The detection of potential recurrent episodes, even in cases where tuberculosis appears to be well-controlled, underscores the need for ongoing and adaptable therapy. These findings endorse the implementation of a comprehensive and adaptable approach to tuberculosis management, which encompasses a blend of medical, behavioral, and systemic interventions to attain long-lasting success in public health.

Despite providing useful insights into TB transmission dynamics, this study has several limitations. First, the model assumes a homogeneous population, which may not fully capture the complexities of real-world transmission patterns. In practice, population heterogeneity, such as differences in age, contact behavior, or socio-economic status, can significantly influence disease spread. In future work, researchers may consider incorporating heterogeneous structures, as

demonstrated in models of other infectious diseases (e.g., [50, 51]). Second, our model does not account for additional infection pathways in TB, such as relapse and reinfection, which are known to contribute to long-term disease persistence and resurgence. Including these mechanisms would provide a more comprehensive understanding of TB dynamics and enhance the model's applicability to diverse epidemiological contexts.

## Use of AI tools declaration

The authors declare they have not used Artificial Intelligence (AI) tools in the creation of this article.

## Data Availibility

The data that been used in this article can be accessed in [37] under license 4.0.

## Acknowledgements

This research is funded by Universitas Indonesia with Riset Kolaborasi Indonesia research grant scheme, 2024 (ID Number: NKB-764/UN2.RST/HKP.05.00/2024).

## Conflict of interest

The authors declare that they have no known competing financial interests or personal relationships that could have appeared to influence the work reported in this paper.

## References

1. D. Aldila, B. L. Fardian, C. W. Chukwu, M. H. N. Aziz, P. Z. Kamalia, Improving tuberculosis control: Assessing the value of medical masks and case detection—a multi-country study with cost-effectiveness analysis, *R. Soc. Open Sci.*, **11** (2024), 231715. https://doi.org/10.1098/rsos.231715
2. Centers for Disease Control and Prevention, Signs and Symptoms of Tuberculosis, 2024, [Online; accessed 10-May-2024]. Available from: https://www.cdc.gov/tb/signs-symptoms/?CDC_AAref_Val=https://www.cdc.gov/tb/topic/basics/signsandsymptoms.htm.
3. C. W. Chukwu, E. Bonyah, M. L. Juga, F. Fatmawati, On mathematical modeling of fractional-order stochastic for tuberculosis transmission dynamics, *Results Control Optim.*, **11** (2023), 100238. https://doi.org/10.1016/j.rico.2023.100238
4. WHO, Global Tuberculosis Report 2022, 2022, [Online; accessed 22-May-2024]. Available from: https://cdn.who.int/media/docs/default-source/hq-tuberculosis/global-tuberculosis-report-2022/global-tb-report-2022-factsheet.pdf?sfvrsn=88f8d76_8&download=true.
5. WHO, Global Tuberculosis Report 2023, 2023, [Online; accessed 25-May-2024]. Available from: https://www.who.int/publications/i/item/9789240061729.
6. WHO, Global Tuberculosis Report 2020, 2020, [Online; accessed 15-May-2024]. Available from: https://www.who.int/publications/i/item/9789240013131.

7. WHO, Global Tuberculosis Report 2019, 2019, [Online; accessed 2-May-2024]. Available from: https://www.who.int/publications/i/item/9789241565714.
8. S. D. Lawn, A. I. Zumla, Tuberculosis, *Lancet*, **378** (2011), 57–72. https://doi.org/10.1016/S0140-6736(10)62173-3
9. B. Song, C. Castillo-Chavez, J. P. Aparicio, Tuberculosis models with fast and slow dynamics: The role of close and casual contacts, *Math. Biosci.*, **180** (2002), 187–205. https://doi.org/10.1016/S0025-5564(02)00112-8
10. R. Xu, J. Yang, X. Tian, J. Lin, Global dynamics of a tuberculosis model with fast and slow progression and age-dependent latency and infection, *J. Biol. Dyn.*, **13** (2019), 675–705. https://doi.org/10.1080/17513758.2019.1683628
11. Stop TB Partnership, Stop TB Partnership: Global Plan to End TB 2023–2030, [Online; accessed 22-May-2024]. Available from: https://www.stoptb.org/news/launched-global-plan-end-tb-2023-2030.
12. Centers for Disease Control and Prevention. TB Disease Treatment: 6- or 9-Month Ripe tb Treatment Regimen, 2023, [Online; accessed 20-May-2024]. Available from: https://www.cdc.gov/tb/webcourses/tb101/page16413.html.
13. A. S. Weichel, Antimycobacterial therapy for tuberculosis, *Am. Fam. Physician*, **61** (2000), 861–862. Available from: https://www.aafp.org/pubs/afp/issues/2000/0201/p861.html.
14. International Union Against Tuberculosis and Lung Disease, Guide for the Clinical and Operational Management of Drug-Resistant Tuberculosis, 2013, [Online; accessed 23-July-2025]. Available from: https://theunion.org/sites/default/files/2020-08/mdr-tbguide_6-19-13_web.pdf.
15. M. Majumder, P. K. Tiwari, S. Pal, Impact of saturated treatments on HIV-TB dual epidemic as a consequence of COVID-19: Optimal control with awareness and treatment, *Nonlinear Dyn.*, **109** (2022), 143–176. https://doi.org/10.1007/s11071-022-07395-6
16. S. Athithan, M. Ghosh, Mathematical modelling of TB with the effects of case detection and treatment, *Int. J. Dyn. Control*, **1** (2013), 223–230. https://doi.org/10.1007/s40435-013-0020-2
17. D. Aldila, J. P. Chávez, K. P. Wijaya, N. C. Ganegoda, G. M. Simorangkir, H. Tasman, et al., A tuberculosis epidemic model as a proxy for the assessment of the novel $M72/AS01_E$ vaccine, *Commun. Nonlinear Sci. Numer. Simul.*, **120** (2023), 107162. https://doi.org/10.1016/j.cnsns.2023.107162
18. Y. D. Zhang, H. F. Huo, H. Xiang, Dynamics of tuberculosis with fast and slow progression and media coverage, *Math. Biosci. Eng.*, **16** (2019), 1150–1170. https://doi.org/10.3934/mbe.2019055
19. K. K. Avilov, A. A. Romanyukha, E. M. Belilovsky, S. E. Borisov, Mathematical modelling of the progression of active tuberculosis: Insights from fluorography data, *Infect. Dis. Modell.*, **7** (2022), 374–386. https://doi.org/10.1016/j.idm.2022.06.007
20. T. Sumner, R. G. White, The predicted impact of tuberculosis preventive therapy: The importance of disease progression assumptions, *BMC Infect. Dis.*, **20** (2020), 880. https://doi.org/10.1186/s12879-020-05592-5

21. K. C. Chong, C. C. Leung, W. W. Yew, B. C. Y. Zee, G. C. H. Tam, M. H. Wang, et al., Mathematical modelling of the impact of treating latent tuberculosis infection in the elderly in a city with intermediate tuberculosis burden, *Sci. Rep.*, **9** (2019), 4869. https://doi.org/10.1038/s41598-019-41256-4
22. S. Bowong, J. J. Tewa, Mathematical analysis of a tuberculosis model with differential infectivity, *Commun. Nonlinear Sci. Numer. Simul.*, **14** (2009), 4010–4021. https://doi.org/10.1016/j.cnsns.2009.02.017
23. L. Liu, Y. Wang, A mathematical study of a tb model with treatment interruptions and two latent periods, *Comput. Math. Methods Med.*, **2014** (2014), 932186. https://doi.org/10.1155/2014/932186
24. D. Okuonghae, B. O. Ikhimwin, Dynamics of a mathematical model for tuberculosis with variability in susceptibility and disease progressions due to difference in awareness level, *Front. Microbiol.*, **6** (2016), 1530. https://doi.org/10.3389/fmicb.2015.01530
25. D. C. Maulana, M. I. Utoyo, U. D. Purwati, C. W. Chukw, Parameter estimation and analysis on sis-seis types model of tuberculosis transmission in east java indonesia, *Commun. Math. Biol. Neurosci.*, **2022** (2022), 114. https://doi.org/10.28919/cmbn/7739
26. E. P. Hafidh, N. Aulida, B. D. Handari, D. Aldila, Optimal control problem from tuberculosis and multidrug resistant tuberculosis transmission model, in *AIP Conference Proceedings 2018*, AIP Publishing, **2023** (2018), 020223. https://doi.org/10.1063/1.5064220
27. O. Diekmann, J. A. P. Heesterbeek, M. G. Roberts, The construction of next-generation matrices for compartmental epidemic models, *J. R. Soc. Interface*, **7** (2010), 873–885. https://doi.org/10.1098/rsif.2009.0386
28. C. Castillo-Chavez, B. Song, Dynamical models of tuberculosis and their applications, *Math. Biosci. Eng.*, **1** (2004), 361–404. https://doi.org/10.3934/mbe.2004.1.361
29. D. Aldila, A. H. Hassan, M. H. N. Aziz, P. Z. Kamalia, An analytical transmission model for evaluating pneumonia vaccination and control strategies, *Healthcare Anal.*, **7** (2025), 100394. https://doi.org/10.1016/j.health.2025.100394
30. D. Aldila, A. H. Hassan, C. W. Chukwu, S. Y. Tchoumi, M. H. N. Aziz, Evaluating vaccination and quarantine for measles intervention strategy in jakarta, indonesia through mathematical modeling, *Partial Differ. Equations Appl. Math.*, **14** (2025), 101191. https://doi.org/10.1016/j.padiff.2025.101191
31. F. A. Oguntolu, O. J. Peter, D. Aldila, G. B. Balogun, O. P. Ogunmola, B. I. Omede, Mathematical analysis of the transmission dynamics of hepatitis B virus, *Braz. J. Phys.*, **55** (2025), 160. https://doi.org/10.1007/s13538-025-01772-3
32. O. J. Peter, D. Aldila, T. A. Ayoola, G. B. Balogun, F. A. Oguntolu, Modeling tuberculosis dynamics with vaccination and treatment strategies, *Sci. Afr.*, **28** (2025), e02647. https://doi.org/10.1016/j.sciaf.2025.e02647
33. D. Aldila, Change in stability direction induced by temporal interventions: A case study of a tuberculosis transmission model with relapse and reinfection, *Front. Appl. Math. Stat.*, **11** (2025), 1541981. https://doi.org/10.3389/fams.2025.1541981

34. H. A. Fatahillah, D. Aldila, Forward and backward bifurcation analysis from an imperfect vaccine efficacy model with saturated treatment and saturated infection, *Jambura J. Biomath.*, **5** (2024), 132–143. https://doi.org/10.37905/jjbm.v5i2.28810

35. D. Aldila, J. P. Chávez, C. W. Chukwu, A. Y. Fathiyah, J. W. Puspita, K. A. D. Setio, et al., Unraveling dengue dynamics with data calibration from palu and jakarta: Optimizing active surveillance and fogging interventions, *Chaos, Solitons Fractals*, **189** (2024), 115729. https://doi.org/10.1016/j.chaos.2024.115729

36. W. M. Liu, Criterion of hopf bifurcations without using eigenvalues, *J. Math. Anal. Appl.*, **182** (1994), 250–256. https://doi.org/10.1006/jmaa.1994.1079

37. World Bank, Incidence of Tuberculosis (per 100,000 people), 2024, [Online; accessed 08-March-2024]. Available from: https://data.worldbank.org/indicator/SH.TBS.INCD.

38. S . Marino, I. B. Hogue, C. J. Ray, D. E. Kirschner, A methodology for performing global uncertainty and sensitivity analysis in systems biology, *J. Theor. Biol.*, **254** (2008), 178–196. https://doi.org/10.1016/j.jtbi.2008.04.011

39. H. Tasman, D. Aldila, P. A. Dumbela, M. Z. Ndii, F. Fatmawati, F. F. Herdicho, et al., Assessing the impact of relapse, reinfection and recrudescence on malaria eradication policy: A bifurcation and optimal control analysis, *Trop. Med. Infect. Dis.*, **7** (2022), 263. https://doi.org/10.3390/tropicalmed7100263

40. B. D. Handari, R. A. Ramadhani, C. W. Chukwu, S. H. A. Khoshnaw, D. Aldila, An optimal control model to understand the potential impact of the new vaccine and transmission-blocking drugs for malaria: A case study in papua and west papua, Indonesia, *Vaccines*, **10** (2022), 1174. https://doi.org/10.3390/vaccines10081174

41. F. Fatmawati, C. W. Chukwu, R. T. Alqahtani, C. Alfiniyah, F. F. Herdicho, Tasmi, A Pontryagin's maximum principle and optimal control model with cost-effectiveness analysis of the COVID-19 epidemic, *Decis. Anal. J.*, **8** (2023), 100273. https://doi.org/10.1016/j.dajour.2023.100273

42. F. Fatmawati, F. F. Herdicho, W. Windarto, C. W. Chukwu, H. Tasman, An optimal control of malaria transmission model with mosquito seasonal factor, *Results Phys.*, **25** (2021), 104238. https://doi.org/10.1016/j.rinp.2021.104238

43. D. Aldila, N. Awdinda, F. Fatmawati, F. F. Herdicho, M. Z. Ndii, C. W. Chukwu, Optimal control of pneumonia transmission model with seasonal factor: Learning from jakarta incidence data, *Heliyon*, **9** (2023), e18096. https://doi.org/10.1016/j.heliyon.2023.e18096

44. C. W. Chukwu, Z. Chazuka, S. Safdar, I. H. Febriana, D. Aldila, Assessing Syphilis transmission among msm population incorporating low and high-risk infection: A modeling study, *Comput. Appl. Math.*, **43** (2024), 205. https://doi.org/10.1007/s40314-024-02669-8

45. M. McAsey, L. Mou, W. Han, Convergence of the forward-backward sweep method in optimal control, *Comput. Optim. Appl.*, **53** (2012) 207–226. https://doi.org/10.1007/s10589-011-9454-7

46. D. Aldila, R. P. Dhanendra, S. H. A. Khoshnaw, J. W. Puspita, P. Z. Kamalia, M. Shahzad, Understanding HIV/AIDS dynamics: Insights from CD4+T cells, antiretroviral treatment, and country-specific analysis, *Front. Public Health*, **12** (2024), 1324858. https://doi.org/10.3389/fpubh.2024.1324858

47. I. H. Febiriana, A. H. Hassan, D. Aldila, Enhancing Malaria control strategy: Optimal control and cost-effectiveness analysis on the impact of vector bias on the efficacy of mosquito repellent and hospitalization, *J. Appl. Math.*, **2024** (2024), 9943698. https://doi.org/10.1155/2024/9943698

48. C. K. Mahadhika, D. Aldila, A deterministic transmission model for analytics-driven optimization of COVID-19 post-pandemic vaccination and quarantine strategies, *Math. Biosci. Eng.*, **21** (2024), 4956–4988. https://doi.org/10.3934/mbe.2024219

49. A. H. Hassan, D. Aldila, M. H. N. Aziz, Optimal control and stability analysis of monkeypox transmission dynamics with the impact of contaminated surfaces, *Front. Appl. Math. Stat.*, **10** (2024), 1372579. https://doi.org/10.3389/fams.2024.1372579

50. W. Li, Y. Wang, J. Cao, M. Abdel-Aty, Dynamics and backward bifurcations of sei tuberculosis models in homogeneous and heterogeneous populations, *J. Math. Anal. Appl.*, **543** (2025), 128924. https://doi.org/10.1016/j.jmaa.2024.128924

51. R. Pastor-Satorras, C. Castellano, P. V. Mieghem, A. Vespignani, Epidemic processes in complex networks, *Rev. Mod. Phys.*, **87** (2015), 925–979. https://doi.org/10.1103/RevModPhys.87.925


AIMS Press